Arbeit zur Erlangung des akademischen Grades Master of Science im Fach Physik

Global Stability of Scalar Potentials in Asymptotically Safe Particle Models

Simon Schreyer

FRIEDRICH-SCHILLER-
UNIVERSITÄT
JENA

Friedrich-Schiller-Universität Jena
Physikalisch-Astronomische Fakultät

Betreut durch: Prof. Dr. Holger Gies

Zweitgutachter: Dr. Luca Zambelli

Contents

1. Introduction

Asymptotic safety has become an important concept in the construction of high-energy complete and consistent quantum field theories [1–8]. In recent years this idea has been used to develop particle physics models that can solve issues of extended particle physics models such as the appearance of Landau-pole singularities [9–11]. An example class of models has been identified by Litim and Sannino in [1]: Gauge-Yukawa theories with many vector-like fermion flavors that become even perturbatively accessible in the Veneziano limit. Whereas many features of the model are accessible by such perturbative means and have been studied to high loop orders [12–14], one important aspect has not been fully explored so far: the stability properties and global existence of the scalar Higgs potentials at large field amplitudes. Since perturbative expansions correspond to small amplitude expansions, these questions need to be addressed by a nonperturbative method. The conditions under which stable potentials can be constructed globally can provide for novel consistency criteria for such models, may help to discover new models and shed light on the question of unitarity of such high-energy-complete quantum field theories.

The structure of the work is as follows. We use methods of the functional renormalization group flow, i.e. the Wetterich equa- tion [15], for nonperturbative investigations of the Gauge-Yukawa theories. The fixed-point potentials, and accordingly the fixed points up to high order are derived via their flow equations in section 2.3.2. The construction of the potential is done implementing analytical methods which are introduced in chapter 3, namely the small- and large-field expansion, the pseudo-spectral method and numerical methods like the shooting method using the framework of Mathematica. These techniques were tested in simpler models like the O(1)-model [16–18] and the Gross-Neveu-model [19, 20] in section 3.2 (both in $d = 3$) before with excellent quantitative results for critical phenomena. At first, in 4.2.1 the small-field expansion (around the origin or the minimum) and the large-field expansion are used to try to construct global fixed-point potentials. This turns out not to be possible due to non overlapping radii of convergence of both expansions. Thus, the computation is tackled implementing a new method, the pseudo-spectral method as done in [19], which uses Chebychev polynomials to approximate the solution of the scalar potential flow equation at the fixed point. This method shows promising results when using it on different theories due to the fast convergence property of the Chebychev polynomials [19, 21–23] and it is targeting in our calculations as well as we show in section 4.2.2. They confirm the existence of both perturbatively calculated interacting UV fixed points and generalize it to operators of higher mass dimension. One of them shows nonperturbatively an accompanying globally stable, bounded fixed-point potential corresponding to the UV fixed point in the symmetry-breaking regime. A fixed-point in the "locally symmetric" regime arises as well and exhibits a global potential which is unbounded from below. Those potentials are investigated regarding their properties and critical phenomena in the sections 4.2.3 and 4.5. Moreover, a fully nonperturbative effect of the non-trivial minimum κ of the fixed-point potential in the symmetry-breaking regime is investigated in 4.4.

2. Physical Foundations

2.1. Functional Renormalization Group and the Wetterich equation

In quantum field theory (QFT), very important objects are correlation functions[1] (or n-point functions) which contain all the physical information, for instance scattering amplitudes. Working in Euclidean space they are defined in the path-integral formalism as

$$\langle \varphi(x_1) \cdots \varphi(x_n) \rangle := \mathcal{N} \int \mathcal{D}\varphi \varphi(x_1) \cdots \varphi(x_n) \mathrm{e}^{-S[\varphi]}, \tag{2.1}$$

where the normalization $\mathcal{N}$ is fixed by the requirement $\langle 1 \rangle = 1$, $\varphi(x_i)$ are the field operators at the spacetime point x_i and $\mathcal{D}\varphi = \prod_x \mathrm{d}\varphi(x)$ the path integral measure. All correlation functions can equally be described by the generating functional

$$Z[J] = \mathrm{e}^{W[J]} = \int \mathcal{D}\varphi \mathrm{e}^{-S[\varphi] + \int \mathrm{d}^D x J\varphi}, \tag{2.2}$$

where we obtain the n-point functions via functional differentiation with respect to the source J. $W[J]$ is the generating functional of the connected correlators which only includes connected diagrams with which we obtain the effective action Γ by a Legendre transformation:

$$\Gamma[\phi] = \sup_J \left(\int \mathrm{d}^d x J\phi - W[J] \right). \tag{2.3}$$

Here, J_{sup} corresponds to the expectation value of φ and d to the dimension of the spacetime. For the effective action an equation, called the Wetterich equation, can be derived (in detail done in [15] or [25]) which has the form

$$\partial_t \Gamma_k[\Phi] = \frac{1}{2} \mathrm{STr} \left[\partial_t R_k \left(\Gamma_k^{(2)}[\Phi] + R_k \right)^{-1} \right], \tag{2.4}$$

with a general field Φ which could include spinors as components, a regulator $R_k(p^2)$, the supertrace STr traces over all indices and incorporates minus signs in fermion loops. Moreover, we use the abbreviation $t = \ln(k/\Lambda)$ with the momentum-shell parameter k, a cutoff Λ and the effective average action Γ_k which is Γ modified by a regulator term. $\Gamma_k^{(2)}[\Phi]$ is the second functional derivative of $\Gamma_k[\Phi]$ with respect to Φ. The effective average action interpolates the bare action $\Gamma_{k\to\Lambda}$ and the full quantum action $\Gamma = \Gamma_{k\to 0}$ where all quantum fluctuations are integrated out. The regulator needs to fulfill the following three requirements:

$$\lim_{q^2/k^2 \to 0} R_k(q) > 0, \tag{2.5}$$

which works as an IR regularization and

$$\lim_{k^2/q^2 \to 0} R_k(q) = 0, \tag{2.6}$$

[1] In this paragraph we only state important facts about QFT. For detailed information consult e.g. Peskin and Schroeder [24].

such that we recover the full effective action in the limit $k \to 0$. At last, we require the regulator to satisfy

$$\lim_{k^2 \to \Lambda \to \infty} R_k(q) \to \infty \tag{2.7}$$

which implies that the functional integral is dominated by the stationary point in this limit. It filters out the classical field configuration of the classical action $\Gamma_{k\to\Lambda} \to S$+const.
At this point, we can name some of the most important properties of the Wetterich equation (2.4). The Wetterich or flow equation is an exact, functional differential equation with one-loop structure for Γ_k where no functional integral has to be performed. It describes the evolution of correlation functions under successive momentum-shell integrations. The regulator $R_k(p^2)$ guarantees an IR regularization because of its occurrence in the denominator and it implements UV regularization because of the $\partial_t R_k$ term since it is dominant near the momentum shell $p^2 \propto k^2$. Furthermore, the peaked structure embodies Wilson's idea of the integration over momentum shells.

2.2. From β functions and fixed points to asymptotic safety

The following paragraph is mainly taken from [26] and [27]. The couplings g_i in the effective average action Γ_k are in general scale dependent which is captured in the β functions[2]

$$\beta_{g_i}\left(\{g_n\}\right) = \partial_t g_i(k) \tag{2.8}$$

where $t = \ln \frac{k}{\Lambda}$ with the energy scale k and the ultraviolet (UV) cutoff Λ. With the abbreviation $\{g_n\}$ we mean that the β function of the coupling g_i is in general dependent on all couplings $g_1, .., g_n$. All the β functions can be extracted from the Wetterich equation as done e.g. in (2.68). This set of equations (i runs over all couplings in Γ_k) thus forms a vector field in the theory space, the so called RG flow. A theory is called scale independent if

$$\beta_{g_i}\left(\{g_n^*\}\right) = 0 \qquad \forall i\,, \tag{2.9}$$

which results in a set of algebraic equations which is solved by the couplings g_i^*. g_i^* refers to the evaluation of the beta functions at the respective fixed-point value of the coupling g_i. (2.9) means that the values for the couplings g_i do not change under a change of the energy scale. Hence, it is valid for all energies. Moreover, this is the definition of a fixed point in theory space which is therefore of particular interest. In general we distinguish two types of fixed points: Gaussian fixed points (GFP) and non-Gaussian fixed points (NGFP) or interacting fixed points. At a GFP all couplings g_i^* vanish whereas at an interacting fixed point at least one $g_i^* \neq 0$ such that there are interactions between the fields. Investigating the vicinity of a fixed point allows for the determination of the critical exponents Θ_I of a theory. The critical exponents are the eigenvalues of the stability matrix

$$B_i^j = \left.\frac{\partial \beta_i}{\partial g_j}\right|_{g^*}\,. \tag{2.10}$$

The flow can be linearized in the vicinity of the fixed point using the stability matrix

$$\beta_{g_i} = B_i^j (g_j - g_j^*) + \mathcal{O}\left((g_j - g_j^*)^2\right) \tag{2.11}$$

with the solution

$$g_i = g_i^* + \sum_I C_I V_i^I \left(\frac{k}{k_0}\right)^{\Theta_I}\,, \tag{2.12}$$

[2] In the β functions we use the dimensionless couplings $\tilde{g}_i = k^{-n} g_i$ (n is the canonical dimension of g_i) which ensures a true scale-independence at the fixed point.

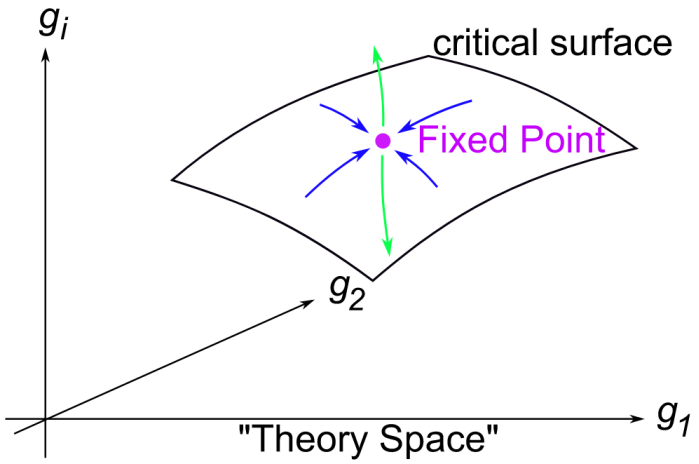

Figure 2.1.: Sketch of the flow towards the ultraviolet (figure taken from [27]). The space of all couplings (theory space) is pictured by the couplings g_1,g_2 and g_i. The blue arrows show the relevant directions, the green ones the irrelevant. The relevant directions lie in the critical hypersurface.

where V_i^I is the eigenvector corresponding to the eigenvalue Θ_I of the stability matrix, C_I is a constant of integration and k_0 is a reference energy scale. Depending on the sign of the eigenvalues we can classify the physical parameters[3].

- Eigendirections where $\mathrm{Re}\{\Theta_I\} < 0$ are called *relevant* directions. Increasing the energy scale k they run into the fixed point (see blue arrows in 2.1).
- Eigendirections where $\mathrm{Re}\{\Theta_I\} > 0$ are called *irrelevant* directions. They run away from the fixed point with increasing k (green arrows in 2.1).
- Eigendirections where $\mathrm{Re}\{\Theta_I\} = 0$ are called *marginal* directions. Here it depends on higher-order terms whether they are marginally relevant or irrelevant.

This classification is related to the predictivity of the theory in the following way. A UV relevant (attractive) direction is infrared (IR) repulsive, meaning that the IR observable value is not determined by the fixed point. Thus, it has to be fixed by experiments and the dimension of the critical hypersurface (all relevant direction lie in this surface) is the number of free parameters of the theory which need to be fixed by experiments. The irrelevant couplings are predictable from the relevant ones. Note that the eigendirections do not simply correspond to the operators entering in the effective action but linear combinations do.
Now we are in the position to introduce the concept of asymptotic safety. In asymptotic safety the system is dominated by an interacting UV fixed point with a finite number of relevant directions. If we increase the energy scale, the trajectory thus ends in the fixed point for arbitrary high energies. This makes the QFT valid at all scales since the couplings are finite even for $\Lambda \to \infty$. Furthermore, in asymptotic safety the IR observables are all dominated by the properties of the UV fixed point. This can be seen from the fact that as we decrease k, the irrelevant directions rapidly approach the critical surface (we go along the inverse direction of the green arrows in figure 2.1). In summary, asymptotic safety is a possibility to achieve that a QFT is well defined at

[3] Due to the asymptotic safety background in which we want to discuss (2.12) we evolve the system towards the ultraviolet.

all energies without being perturbatively renormalizable. This could lead to high-energy consistent, UV complete QFTs which are of particular interest and thus could be candidates for physics beyond the standard model. Note that a UV fixed point does not guarantee that the theory is stable or unitary. For this, e.g. the global stability of the potential in the scalar sector is needed which will be investigated in this work.

2.3. Gauge-Yukawa theories in four dimensions

In particle physics we aim at fundamental, high-energy complete QFTs which could be candidates beyond the standard model. Those QFTs should contain the standard model as a low energy effective field theory. Recently, a new class of Gauge-Yukawa theories was discovered by Litim and Sannino in [1] (and earlier papers) whose high-energy behavior is controlled by an interacting fixed point which makes the class asymptotically safe as described in section 2.2. Furthermore, the class has the interesting property of being perturbatively accessible which gives us an opportunity to compare nonperturbative FRG results with perturbative calculations. In the following we introduce the Gauge-Yukawa class and review its perturbative results (which are computed in [1]).

The class of Gauge-Yukawa theories contains $SU(N_c)$ gauge fields A_μ^a combined in the field strength tensor $F_{\mu\nu}^a$, with $a \in \{1,..,{N_c}^2-1\}$, N_f flavors of fermions Q_i ($i \in \{1,..,,N_f\}$) in the fundamental representation and an $N_f \times N_f$ complex scalar field H which is uncharged under the gauge group. The action is the sum of the Yang-Mills like term, fermionic kinetic term, Yukawa coupling, scalar kinetic term and self-interaction terms of the scalar field which forms the Lagrangian $\mathcal{L}_M$ in Minkowski space:

$$\begin{aligned}\mathcal{L}_M = &-\frac{1}{2}\operatorname{Tr} F^{\mu\nu}F_{\mu\nu} + \operatorname{Tr}\overline{Q}i\not{D}Q + y\operatorname{Tr}\left(\overline{Q}_L H Q_R + \overline{Q}_R H^\dagger Q_L\right) + \\ &+ \operatorname{Tr}\left(\partial_\mu H^\dagger \partial^\mu H\right) - u\operatorname{Tr}\left(H^\dagger H\right)^2 - v\left(\operatorname{Tr} H^\dagger H\right)^2,\end{aligned} \tag{2.13}$$

where g, y, u, v are the accompanying coupling constants. The trace in the different terms is understood to be the sum over both the color and flavor indices. Furthermore, we use here the decomposition into left- and right-handed fermions Q_L, Q_R with $Q_{L/R} = \frac{1}{2}\left(1 \pm \gamma_5\right)Q$. Note that due to the fact that the scalar field is a complex matrix, the terms $\operatorname{Tr}\left(H^\dagger H\right)^2$ and $\left(\operatorname{Tr} H^\dagger H\right)^2$ are different invariants. To apply the machinery of Wetterich's equation to (2.13), it is convenient to transform (2.13) from Minkowski space into Euclidean space. In Euclidean space we want to work with a hermitean $2N_f \times 2N_f$ scalar field[4] ϕ. To perform the transformation we use the following conventions: In Minkowksi space $\{\gamma_\mu, \gamma_\nu\} = 2\eta_{\mu\nu}\mathbb{1}_{4\times4}$ with $\eta_{\mu\nu} = \operatorname{diag}(+,-,-,-)$ the chiral representation is

$$\gamma^0 = \begin{pmatrix} 0 & \mathbb{1}_{2\times2} \\ \mathbb{1}_{2\times2} & 0 \end{pmatrix}, \qquad \gamma^i = \begin{pmatrix} 0 & \sigma^i \\ -\sigma^i & 0 \end{pmatrix}, \quad \text{such that } \left(\gamma^0\right)^\dagger = \gamma^0 \text{ and } \left(\gamma^i\right)^\dagger = -\gamma^i, \tag{2.14}$$

where σ^i ($i \in \{1,2,3\}$) are the usual Pauli-matrices. The Dirac conjugation in Minkowski space is defined as $\overline{\Psi} = \Psi^\dagger\gamma^0$. In Euclidean space $\{\gamma_\mu, \gamma_\nu\} = 2\delta_{\mu\nu}\mathbb{1}_{4\times4}$ where we think of x_4 as the Euclidean time direction (related to Minkowski time t by a Wick rotation) the chiral representation

[4] This is not mandatory but it is done for "historical" reasons in the course of this work. In [28] a quite similar problem is tackled in this manner which was the starting point of the present thesis.

reads

$$\gamma^4 = \begin{pmatrix} 0 & \mathbb{1}_{2\times 2} \\ \mathbb{1}_{2\times 2} & 0 \end{pmatrix}, \qquad \gamma^i = \begin{pmatrix} 0 & -i\sigma^i \\ i\sigma^i & 0 \end{pmatrix}, \quad \text{such that } \left(\gamma^4\right)^\dagger = \gamma^4 \text{ and } \left(\gamma^i\right)^\dagger = \gamma^i. \tag{2.15}$$

Considering ψ and $\overline{\psi}$ as independent degrees of freedom, we define a generalized hermitean conjugation as $\overline{\Psi} := -i\Psi^\dagger\gamma^4$. From these definitions, it can be easily shown that the Lagrangian in Euclidean space reads

$$\mathcal{L} \equiv \mathcal{L}_E = \frac{1}{2}\operatorname{Tr} F^{\mu\nu}F_{\mu\nu} + \bar{\chi}^i i\not{D}\chi^i + i h_\phi \bar{\chi}^i \phi^{ij}\chi^j + \frac{1}{2}\left(\partial_\mu \phi^{ij}\partial^\mu \phi^{ji}\right) + U(\phi^2), \tag{2.16}$$

where the scalar field

$$\phi = \begin{pmatrix} 0_{N_\mathrm{f}\times N_\mathrm{f}} & H \\ H^\dagger & 0_{N_\mathrm{f}\times N_\mathrm{f}} \end{pmatrix}, \tag{2.17}$$

is hermitean and the fermion fields are defined as $\chi = (Q_L, Q_R)^\mathrm{T}$ and $\bar{\chi} = (\overline{Q}_L, \overline{Q}_R)$ such that $i, j \in 1, .., 2N_\mathrm{f}$. The scalar self interaction terms are included into the potential U and will occur when a truncation of the form

$$U(\phi^2) = \begin{cases} \overline{m}_\phi^2\rho + \frac{\lambda_1}{2}\rho^2 + \lambda_2\tau & \text{symmetric regime} \\ \frac{\lambda_1}{2}(\rho-\rho_0)^2 + \lambda_2\tau & \text{symmetry-breaking regime,} \end{cases} \tag{2.18}$$

is chosen. Here

$$\rho = \frac{1}{2}\operatorname{Tr}\phi^2, \qquad \tau = \frac{1}{2}\operatorname{Tr}\left(\frac{1}{2}\phi^2 - \frac{\rho}{N_\mathrm{f}}\right)^2, \tag{2.19}$$

are the conventions chosen for the scalar self interaction invariants. The coupling constants u, v in (2.13) correspond to λ_1, λ_2 in (2.16). Let us note here that there are of course higher order invariants constructible from $\tau_n \propto \operatorname{Tr}(\phi^2/2 - \rho/N_\mathrm{f})^n$ for $n \geq 3$ at higher field orders which we suppress in the following.[5] The relation between the invariants u, v and λ_1, λ_2 is given by

$$u = \frac{\lambda_2}{4}, \qquad v = \frac{\lambda_1}{2} - \frac{\lambda_2}{4N_\mathrm{f}}. \tag{2.21}$$

Each term in (2.16) fulfills the Osterwalder-Schrader reflection positivity [30, 31] (OSRP). The OSRP is a condition for a Wick rotation between Minkowskian and Euclidean field theories. Hence, OSRP is an important check for the transformation to Euclidean space.

2.3.1. Perturbative results

In this section we give a short overview of the results in [1] where the above model (2.13) is discussed in the Veneziano limit

$$\epsilon = \frac{N_\mathrm{f}}{N_\mathrm{c}} - \frac{11}{2} \ll 1 \tag{2.22}$$

[5] The number of linearly independent invariants depends on the number of fermions N_f of the system, i.e. there are N_f invariants [29]. For example the invariant τ_3 is given by

$$\tau_3 = \frac{1}{16}\operatorname{Tr}\phi^6 - \frac{3}{N_\mathrm{f}}\rho\tau - \frac{\rho^3}{2{N_\mathrm{f}}^2}, \tag{2.20}$$

which is only expressible in terms of the lower order invariants ρ and τ if $N_\mathrm{f} = 1$ or $N_\mathrm{f} = 2$. It shows that in the cases $N_\mathrm{f} > 2$ the invariant τ_3 exists and differs from the others.

where perturbation theory is applicable. The first few possible (N_c, N_f) configurations corresponding to a decreasing set of ϵ values are

$$(N_c, N_f) = (5,28),(7,39),(9,50),(11,61),(13,72),(15,83)\cdots,(53,292),\cdots, \tag{2.23}$$

such that

$$\epsilon = \frac{1}{10},\frac{1}{14},\frac{1}{18},\frac{1}{22},\frac{1}{26},\frac{1}{30},\cdots,\frac{1}{106},\cdots \tag{2.24}$$

With the abbreviations

$$\alpha_g = \frac{g^2 N_c}{(4\pi)^2},\quad \alpha_y = \frac{y^2 N_c}{(4\pi)^2},\quad \alpha_h = \frac{u N_f}{(4\pi)^2},\quad \alpha_v = \frac{v N_f^2}{(4\pi)^2}, \tag{2.25}$$

the perturbative β functions for the quartic couplings α_h and α_v to one-loop order, the β functions for the Yukawa coupling α_y to two-loop order and gauge coupling α_g to three-loop order read (from [12–14])

$$\beta_h = -(11+2\epsilon)\alpha_y^2 + 4\alpha_h(\alpha_y + 2\alpha_h), \tag{2.26}$$

$$\beta_v = 12\alpha_h^2 + 4\alpha_v(\alpha_v + 4\alpha_h + \alpha_y), \tag{2.27}$$

$$\begin{aligned}\beta_y =& \alpha_y\left\{(13+2\epsilon)\alpha_y - 6\alpha_g\right\} + \\ &+ \alpha_y\left\{\frac{20\epsilon-93}{6}\alpha_g^2 + (49+8\epsilon)\alpha_g\alpha_y - \left(\frac{385}{8}+\frac{23}{2}\epsilon+\frac{\epsilon^2}{2}\right)\alpha_y^2 - (44+8\epsilon)\alpha_y\alpha_h + 4\alpha_h^2\right\},\end{aligned} \tag{2.28}$$

$$\begin{aligned}\beta_g =& \alpha_g^2\left\{\frac{4}{3}\epsilon + \left(25+\frac{26}{3}\epsilon\right)\alpha_g - 2\left(\frac{11}{2}+\epsilon\right)^2\alpha_y\right\} \\ &+ \alpha_g^2\left\{\left(\frac{701}{6}+\frac{53}{3}\epsilon-\frac{112}{27}\epsilon^2\right)\alpha_g^2 - \frac{27}{8}(11+2\epsilon)^2\alpha_g\alpha_y + \frac{1}{4}(11+2\epsilon)^2(20+3\epsilon)\alpha_y^2\right\}.\end{aligned} \tag{2.29}$$

Note that this set of β functions displays a Gaussian fixed point $(\alpha_g^*, \alpha_y^*, \alpha_h^*, \alpha_v^*) = (0,0,0,0)$. Furthermore, the β functions $\beta_g, \beta_y, \beta_h$ are independent of the double-trace scalar coupling α_v, meaning the dynamics of α_v decouples from the system. It does not influence the build-up of the asymptotically safe UV fixed point in the $(\alpha_g, \alpha_y, \alpha_h)$ sector. The evolution of α_v and its fixed points are primarily driven by the Yukawa and the single-trace coupling. Besides the Gaussian fixed point the system (2.26)-(2.29) exhibits interacting UV fixed points making the system asymptotically safe. In the gauge-Yukawa subsector the fixed-point couplings are uniquely determined whereas in the scalar sector multiple fixed-point values arise. One of those fixed points turns out to correspond to a potential quartic in the scalar field amplitude which is perturbatively bounded from below. This makes it physically the most interesting one. For the full system the NGFP reads in an numerical expansion in ϵ as follows

$$\alpha_g^* = 0.4561\epsilon + 0.7808\epsilon^2 + 3.112\epsilon^3 + \mathcal{O}(\epsilon^4), \tag{2.30}$$

$$\alpha_y^* = 0.2105\epsilon + 0.5082\epsilon^2 + 2.100\epsilon^3 + \mathcal{O}(\epsilon^4), \tag{2.31}$$

$$\alpha_{h1}^* = 0.1998\epsilon + 0.5042\epsilon^2 + 2.045\epsilon^3 + \mathcal{O}(\epsilon^4), \tag{2.32}$$

$$\alpha_{v1}^* = -0.1373\epsilon + \mathcal{O}(\epsilon^2). \tag{2.33}$$

We observe that the fixed-point values are perturbatively small in the Veneziano limit (2.22) (the smaller ϵ the better the approximation). Equivalently, we can express the fixed point using (2.21)

and (2.25) in terms of the couplings (g^2, h_ϕ^2, λ_1, λ_2) which results in

$$h_\phi^{2*} = \frac{(4\pi)^2}{N_\mathrm{c}}(0.2105\epsilon + 0.5082\epsilon^2 + 2.100\epsilon^3 + \mathcal{O}(\epsilon^4)), \tag{2.34}$$

$$g^{2*} = \frac{(4\pi)^2}{N_\mathrm{c}}(0.4561\epsilon + 0.7828\epsilon^2 + 3.112\epsilon^3 + \mathcal{O}(\epsilon^4)), \tag{2.35}$$

$$\lambda_{1,1}^* = \frac{2(4\pi)^2}{{N_\mathrm{f}}^2}(0.0625\epsilon + 0.5042\epsilon^2 + 2.045\epsilon^3 + \mathcal{O}(\epsilon^4)), \tag{2.36}$$

$$\lambda_{2,1}^* = \frac{4(4\pi)^2}{N_\mathrm{f}}(0.1998\epsilon + 0.5042\epsilon^2 + 2.045\epsilon^3 + \mathcal{O}(\epsilon^4)). \tag{2.37}$$

For this fixed point, we can compute the critical exponents and the relevant and irrelevant directions as explained in section 2.2. The critical exponents can be given in an expansion in ϵ as well. They read

$$\Theta_1 = -0.608\epsilon^2 + 0.707\epsilon^3 + 2.283\epsilon^4 + \cdots, \tag{2.38}$$

$$\Theta_2 = 2.737\epsilon + 6.676\epsilon^2 + \cdots, \tag{2.39}$$

$$\Theta_3 = 4.039\epsilon + 14.851\epsilon^2 + \cdots, \tag{2.40}$$

$$\Theta_4 = 2.941\epsilon + \cdots, \tag{2.41}$$

with the negative eigenvalue corresponding to the only relevant direction. Let us name the other possible fixed point of the full system of couplings which corresponds to a perturbative scalar potential which is unbounded from below. It is called $(\alpha_g^*, \alpha_y^*, \alpha_{h1}^*, \alpha_{v2}^*)$ and is located at

$$\alpha_{v2}^* = -0.8723\epsilon + \mathcal{O}(\epsilon^2) \quad \text{or} \quad \lambda_{1,2}^* = 2\frac{(4\pi)^2}{{N_\mathrm{f}}^2} \times (-0.6725\epsilon + \mathcal{O}(\epsilon^2)). \tag{2.42}$$

The other values remain unchanged. This fixed point has the same critical exponents except for Θ_4. Θ_4 changes sign[6]. Moreover, inserting (2.30) and (2.31) into the β function (2.26) of the single-trace coupling α_h we find a second possible fixed-point value for the coupling α_h:

$$\alpha_{h2}^* = -(\sqrt{23}+1)\frac{\epsilon}{19} + \mathcal{O}(\epsilon^2) \quad \text{or} \quad \lambda_{2,2}^* = 4(4\pi)^2 N_\mathrm{f} \times (0.3050\epsilon + \mathcal{O}(\epsilon^2) \tag{2.43}$$

but inserting α_{h2}^* into (2.27) does not give a legitimate solution α_v^* since the condition $\epsilon \ll 1$ is violated. Thus, we do not end up in a fixed point for the full system. To sum up, perturbatively there are two fixed-point values for α_v and α_h where the combination $(\alpha_g^*, \alpha_y^*, \alpha_{h1}^*, \alpha_{v1}^*)$ exhibits a fixed point which shows a scalar field potential which is bounded from below (one relevant direction) and one combination $(\alpha_g^*, \alpha_y^*, \alpha_{h1}^*, \alpha_{v2}^*)$ which results in a potential which is unbounded from below (two relevant directions). The other two combinations do not build up a controlled fixed point in the full system. At this point it is important to stress once again that those results are valid perturbatively up to H^4. But perturbative results cannot make any statement about the global existence of those fixed-point potentials since large field amplitudes can compensate for small couplings. For large field amplitudes which are important for the global existence (higher order operators have a non-trivial influence on the stability) the results of this section are not valid. Due to this reason nonperturbative methods like FRG need to be used in order to answer the question of global stability.

[6] This is only true for perturbative calculations in this nomenclature since only then the coupling α_v appears only quadratically in the β functions to all orders.

2.3.2. Flow equations

In this section we derive the flow equation for the scalar potential following from Wetterich's equation (2.4) and list the other flow equations which are important for the calculation of the fixed point and its potential. Those equations are derived in detail in [29]. Let us start with an approximation (truncation) of the full effective average action:

$$\Gamma_k = \int \mathrm{d}^d x \left[\frac{Z_{A,k}}{4} F^{a\mu\nu} F^a_{\mu\nu} + Z_{\chi,k} \bar{\chi}^{a,i} i \not{D} \chi^{a,i} + i h_{\phi,k} \bar{\chi}^{a,i} \phi^{ij} \chi^{a,j} + \frac{Z_{\phi,k}}{2} \left(\partial_\mu \phi^{ij} \partial^\mu \phi^{ji} \right) + U_k(\phi^2) \right], \tag{2.44}$$

where $Z_{A,k}, Z_{\chi,k}, Z_{\phi,k}$ are wave function renormalizations. Every coupling in (2.44) is explicitly written down as energy scale k dependent which also holds for the couplings hidden inside $U_k(\phi^2)$. In our case, the potential will be truncated as

$$U_k(\phi^2) = \begin{cases} \overline{m}^2_{\phi,k} \rho + \frac{\lambda_{1,k}}{2} \rho^2 + \lambda_{2,k} \tau & \text{symmetric regime} \\ \frac{\lambda_{1,k}}{2} (\rho - \rho_{0,k})^2 + \lambda_{2,k} \tau & \text{symmetry-breaking regime,} \end{cases} \tag{2.45}$$

Since χ and $\bar{\chi}$ are implicitly written in left and right handed components, we work here with Weyl spinors. We obtain the flow equation for the scalar potential from the Wetterich equation by

$$\partial_t \Gamma_k[\chi, \bar{\chi}, \phi]\big|_{\chi=\bar{\chi}=0, \phi=\phi_0} = \Omega \, \partial_t U_k = \frac{1}{2} \mathrm{STr} \left[\partial_t R_k \left(\Gamma^{(2)}_k[\chi, \bar{\chi}, \phi] + R_k \right)^{-1} \right] \Big|_{\chi=\bar{\chi}=0, \phi=\phi_0}. \tag{2.46}$$

Here, Ω is the spacetime volume. To compute the RHS of this equation, we first have to derive the explicit form of the fluctuation matrix $\Gamma^{(2)}_k[\chi, \bar{\chi}, \phi]$. In momentum space, this is done performing functional derivatives the following way: (see e.g. [21])

$$\Gamma^{(2)}_k(p,q) \coloneqq \begin{pmatrix} \frac{\vec{\delta}}{\delta H^{ab}_R(-p)} \\ \frac{\vec{\delta}}{\delta H^{ab}_I(-p)} \\ \frac{\vec{\delta}}{\delta (\chi^{a,i})^{\mathrm{T}}(-p)} \\ \frac{\vec{\delta}}{\delta \bar{\chi}^{a,i}(p)} \end{pmatrix} \Gamma_k \left(\frac{\overleftarrow{\delta}}{\delta H^{rs}_R(q)}, \frac{\overleftarrow{\delta}}{\delta H^{rs}_I(q)}, \frac{\overleftarrow{\delta}}{\delta \chi^{b,j}(q)}, \frac{\overleftarrow{\delta}}{\delta (\bar{\chi}^{b,j})^{\mathrm{T}}(-q)} \right), \tag{2.47}$$

where $a, b, r, s \in 1, .., N_\mathrm{f}$ are indices in spinor space and $i, j \in 1, .., N_\mathrm{c}$ indices corresponding to the gauge space. H_R represents the real part of the complex scalar field H and H_I the imaginary part. Appendix A.1 presents the functional derivatives of the scalar sector in detail which is as well called the mass spectrum of scalar fluctuations. It gives the component $\left(\Gamma^{(2)}_k\right)_{11}$ and $\left(\Gamma^{(2)}_k\right)_{22}$ (off diagonal terms vanish)[7]. There are two more non-vanishing components, namely $\left(\Gamma^{(2)}_k\right)_{34}$ and $\left(\Gamma^{(2)}_k\right)_{43}$ due to the kinetic and Yukawa contributions. They result in

$$\left(\Gamma^{(2)}_k\right)_{34} = \left(-Z_{\chi,k} \delta_{ab} \not{p}^{\mathrm{T}} - \mathrm{i} \, h_{\phi,k} \phi_0^{ab}(p-q) \right) \delta_{pq} \delta_{ij}, \tag{2.48}$$

$$\left(\Gamma^{(2)}_k\right)_{43} = \left(-Z_{\chi,k} \delta_{ab} \not{p} + \mathrm{i} \, h_{\phi,k} \phi_0^{ab}(p-q) \right) \delta_{pq} \delta_{ij}. \tag{2.49}$$

[7] A more general result for the mass spectrum is computed in appendix A.2 where we have also included second derivatives with respect to τ.

Defining the regulator as

$$R_k(p) = \begin{pmatrix} Z_{\phi,k} p^2 r_{kB}(p)\delta_{as}\delta_{br} & 0 & 0 & 0 \\ 0 & Z_{\phi,k} p^2 r_{kB}(p)\delta_{as}\delta_{br} & 0 & 0 \\ 0 & 0 & 0 & -Z_{\chi,k} \not{p}^{\mathrm{T}} r_{kF}(-p)\delta_{ab}\delta_{ij} \\ 0 & 0 & -Z_{\chi,k} \not{p} r_{kF}(p)\delta_{ab}\delta_{ij} & 0 \end{pmatrix} \delta_{pq} \tag{2.50}$$

with the dimensionless cut-off functions $r_{kB}(p)$ and $r_{kF}(p)$ fulfilling the property $r_k = r(p^2/k^2)$. We are now in the position to derive $\left(\Gamma_k^{(2)}[\chi,\bar{\chi},\phi] + R_k\right)^{-1}$ which has the non-vanishing components

$$\left(\Gamma_k^{(2)}\right)_{11} = \frac{1}{Z_{\phi,k} P(p) + M_{R,abrs}}, \tag{2.51}$$

$$\left(\Gamma_k^{(2)}\right)_{22} = \frac{1}{Z_{\phi,k} P(p) + M_{I,abrs}}, \tag{2.52}$$

$$\left(\Gamma_k^{(2)}\right)_{34} = \frac{-Z_{\chi,k}(1 + r_{kF}(p))\not{p}\delta_{ab} + \mathrm{i}\, h_\phi \phi_0^{ab}}{Z_{\chi,k}^2 P_F(p) + h_\phi^2 \phi_0^2}\delta_{pq}\delta_{ij}, \tag{2.53}$$

$$\left(\Gamma_k^{(2)}\right)_{43} = \frac{-Z_{\chi,k}(1 + r_{kF}(p))\not{p}^{\mathrm{T}}\delta_{ab} - \mathrm{i}\, h_\phi \phi_0^{ab}}{Z_{\chi,k}^2 P_F(p) + h_\phi^2 \phi_0^2}\delta_{pq}\delta_{ij}, \tag{2.54}$$

where $M_{R,abrs}$ and $M_{I,abrs}$ are two parts of the scalar mass spectrum (see appendix A.1), $P_F(p) = p^2(1 + r_{kF}(p))^2$ and $P(p) = p^2(1 + r_{kB}(p))$. Note that the expressions (2.51)-(2.54) themselves are matrices which can be rewritten using the spectral theorem in terms of their eigenvalues. For the scalar sector, they are computed in appendix A.1 and for the fermionic sector they are just the eigenvalues of ϕ_0^2. To proceed, we choose a specific configuration of the scalar field. Since the potential depends only on ρ and τ (in our truncation (2.18)) it is sufficient to evaluate the flow equation on a two dimensional subspace of all possible scalar configurations. Hence, we might choose

$$H^{ab} = \frac{1}{\sqrt{2}}(H_R^{ab} + \mathrm{i}\, H_I^{ab}) \coloneqq m \times \mathrm{diag}(\varepsilon, \underbrace{+1., .., +1}_{N_\mathrm{f}-1 \text{ times}}) \coloneqq \varphi^a \delta^{ab}, \tag{2.55}$$

with the real parameters m, ε and no sum over a is understood in the last part. They are connected to ρ, τ via (2.19):

$$\tau = \frac{m^4}{2}\frac{N_\mathrm{f}-1}{N_\mathrm{f}}(1-\varepsilon)^2, \qquad \rho = m^2(N_\mathrm{f} - 1 + \varepsilon^2), \tag{2.56}$$

$$m^2 = \frac{\rho}{N_\mathrm{f}}\left(1 - \sqrt{\frac{4N_\mathrm{f}}{N_\mathrm{f}-1}\frac{\tau}{\rho^2}}\right), \qquad \varepsilon^2 = 1 + N_\mathrm{f}\left(\frac{1}{1 - \sqrt{\frac{4N_\mathrm{f}}{N_\mathrm{f}-1}\frac{\tau}{\rho^2}}} - 1\right). \tag{2.57}$$

With this simplification, we are able to compute the eigenvalues of ϕ_0^2 which result in the eigenvalue m^2 (degeneracy: $2(N_\mathrm{f}-1)$) and $m^2\varepsilon^2$ (degeneracy: 2). For the scalar sector the mass spectrum is given in table 2.1. Let us in the next step of our derivation for the flow equation of the

Table 2.1.: Scalar mass spectrum (eigenvalues $\mathfrak{m}^2$ of $M_{R,abrs}$ and $M_{I,abrs}$), $U_{k,\tau} \equiv \frac{\partial U_k}{\partial \tau}$.

Eigenvalue	Degeneracy
$U'_k + \frac{m^2}{2} U_{k,\tau} \frac{1-N_\mathrm{f}}{N_\mathrm{f}} \left(1-\varepsilon^2\right)$	1
$U'_k + \frac{m^2}{2} U_{k,\tau} \frac{1-\varepsilon^2}{N_\mathrm{f}}$	${N_\mathrm{f}}^2 - 2N_\mathrm{f} + 1$
$U'_k + \frac{m^2}{2} U_{k,\tau} \left(\varepsilon^2 \pm \varepsilon + \frac{1-\varepsilon^2}{N_\mathrm{f}}\right)$	$2N_\mathrm{f} - 2 + 2N_\mathrm{f} - 2$
$U'_k + \frac{m^2}{2} U_{k,\tau} \left(2 + \frac{1-\varepsilon^2}{N_\mathrm{f}}\right)$	${N_\mathrm{f}}^2 - 2N_\mathrm{f}$
$U'_k + \frac{m^2}{4N_\mathrm{f}} \Big\{ 4N_\mathrm{f}(N_\mathrm{f}-1) U''_k + (4-N_\mathrm{f}) U_{k,\tau} + \left[4N_\mathrm{f} U''_k + (3N_\mathrm{f}-4) U_{k,\tau}\right] \varepsilon^2$ $\pm \Big[\left(4N_\mathrm{f}(N_\mathrm{f}-1) U''_k + (N_\mathrm{f}+2) U_{k,\tau}\right)^2$ $+2\big(16{N_\mathrm{f}}^2(N_\mathrm{f}-1) U''^2_k - 4N_\mathrm{f}(N_\mathrm{f}+2)(3N_\mathrm{f}-2) U''_k U_{k,\tau}$ $-(3{N_\mathrm{f}}^2 - 4N_\mathrm{f} + 4) U^2_{k,\tau}\big)\varepsilon^2 + \left(4N_\mathrm{f} U''_k + (3N_\mathrm{f}-2) U_{k,\tau}\right)^2 \varepsilon^4 \Big]^{1/2} \Big\}$	$1+1$

scalar potential evaluate the supertrace:

$$
\begin{aligned}
\Omega\, \partial_t U_k &= \frac{1}{2} \mathrm{STr} \left[\partial_t R_k \left(\Gamma_k^{(2)}[\chi, \bar{\chi}, \phi] + R_k \right)^{-1} \right] \Big|_{\chi=\bar{\chi}=0, \phi=\phi_0} \\
\partial_t U_k &= \frac{1}{2} \int_p \sum_{i=1}^{2{N_\mathrm{f}}^2} \frac{\partial_t R_{kB}(p)}{Z_{\phi,k} P(p) + \mathfrak{m}_i^2} - \frac{d_W}{2} \int_p \sum_{i=1}^{2N_\mathrm{f}} \underbrace{\partial_t \left(-Z_{\chi,k} r_{kF}(p)\right)}_{\partial_t R_{kF}} \frac{-2 Z_{\chi,k} (1 + r_{kF}(p)) p^2}{Z^2_{\chi,k} P_F(p) + h^2_\phi \mathfrak{m}_i^2} \\
&= \frac{1}{2 Z_{\phi,k}} \int_p \sum_{i=1}^{2{N_\mathrm{f}}^2} \frac{\partial_t R_{kB}(p)}{P_(p) + Z^{-1}_{\phi,k} \mathfrak{m}_i^2} - \frac{d_W N_\mathrm{c}}{Z_{\chi,k}} \int_p \partial_t \left(Z_{\chi,k} r_{kF}(p)\right) P_F(p) \Big[\frac{2\,(N_\mathrm{f}-1)}{P_F(p) + Z^{-2}_{\chi,k} h^2_\phi m^2} + \\
&\quad + \frac{2}{P_F(p) + Z^{-2}_{\chi,k} h^2_\phi m^2 \varepsilon^2} \Big].
\end{aligned}
\tag{2.58}
$$

We have used the eigenvalues of the corresponding matrices, the abbreviation $\int_p \equiv \int \mathrm{d}^d p/(2\pi)^d$, a symmetry of the cut-off function $r_k(-p) = r_k(p)$, the identity $\not{p}\not{p} = d_W p^2$ with the dimension of the Weyl-matrices $d_W = d_\gamma/2$ and $\mathfrak{m}_i^2$ as the eigenvalues from table 2.1. Moreover, the trace over the color indices gives a factor of N_c in the fermionic sector and the trace over the spacetime points gives the spacetime volume Ω which cancels out. In the final step, we rewrite (2.58) into dimensionless form and express the potential in terms of its invariants ρ and τ. We use the dimensionless quantities denoted with a tilde[8]

$$
\widetilde{\phi}^{ab} = Z^{1/2}_{\phi,k} \phi^{ab}, \qquad \widetilde{\rho} = Z_{\phi,k} k^{2-d} \rho, \qquad \widetilde{\tau} = Z^2_{\phi,k} k^{2(2-d)} \tau, \tag{2.59}
$$

$$
\widetilde{\chi}^a = Z^{1/2}_{\chi,k} \chi^a, \qquad \widetilde{\bar{\chi}}^a = Z^{1/2}_{\chi,k} \bar{\chi}^a, \qquad \widetilde{h}^2_\phi = Z^{-1}_\phi Z^{-2}_{\chi,k} k^{d-4} h^2_{\phi,k}, \tag{2.60}
$$

$$
\kappa = Z_{\phi,k} k^{2-d} \rho_{0,k}, \qquad \bar{\varepsilon} = Z^{-1}_{\phi,k} k^2 \overline{m}^2_\phi, \qquad \widetilde{\lambda}_{1/2} = Z^{-2}_{\phi,k} k^{4-d} \lambda_{1/2,k}, \tag{2.61}
$$

[8] In order to not get confused with definitions, remember that $\epsilon = N_\mathrm{f}/N_\mathrm{c} - 11/2$ is the small parameter in perturbative calculations, that we have parameterized the scalar field configurations with the parameter ε and that $\bar{\varepsilon}$ is the dimensionless mass parameter.

Hence, the parameters of the two dimensional subspace of the scalar configurations transform as

$$\widetilde{\varepsilon}^2 = \varepsilon^2, \qquad \widetilde{m}^2 = Z_{\phi,k} k^{2-d} m^2, \tag{2.62}$$

and

$$u(\widetilde{\rho},\widetilde{\tau}) = k^{-d} U_k\left(Z_{\phi,k}^{-1} k^{d-2}\widetilde{\rho}, Z_{\phi,k}^{-2} k^{2(d-2)}\widetilde{\tau}\right). \tag{2.63}$$

Using the definitions of the threshold functions (see appendix B) (2.58) can be written in the compact form

$$\begin{aligned}\partial_t u =& -d u + (d-2+\eta_\phi)\widetilde{\rho} u' + (2d-4+2\eta_\phi)\widetilde{\tau} u_{,\widetilde{\tau}} + 2 v_d \sum_{i=1}^{2N_\mathrm{f}^2} l_0^d\left(\mathfrak{m}_i^2;\eta_\phi\right) + \\ & - 2 v_d d_\gamma N_\mathrm{c}\left[(N_\mathrm{f}-1) l_0^{(F)d}\left(\widetilde{m}^2\widetilde{h}_\phi^2;\eta_\chi\right) + l_0^{(F)d}\left(\widetilde{m}^2\varepsilon^2\widetilde{h}_\phi^2;\eta_\chi\right)\right].\end{aligned} \tag{2.64}$$

Working with a linear cut-off, the threshold functions can be integrated analytically (see appendix B), yielding

$$\begin{aligned}\partial_t u =& -d u + (d-2+\eta_\phi)\widetilde{\rho} u' + (2d-4+2\eta_\phi)\widetilde{\tau} u_{,\widetilde{\tau}} + \frac{4 v_d}{d}\left(1-\frac{\eta_\phi}{d+2}\right)\sum_{i=1}^{2N_\mathrm{f}^2}\frac{1}{1+\mathfrak{m}_i^2} + \\ & - \frac{4 v_d}{d} d_\gamma N_\mathrm{c}\left(1-\frac{\eta_\chi}{d+1}\right)\left[\frac{N_\mathrm{f}-1}{1+\widetilde{m}^2\widetilde{h}_\phi^2} + \frac{1}{1+\widetilde{m}^2\varepsilon^2\widetilde{h}_\phi^2}\right].\end{aligned} \tag{2.65}$$

We have used the abbreviations $u \equiv u(\widetilde{\rho},\widetilde{\tau})$, $u' \equiv \partial u/\partial\widetilde{\rho}$, $u_{,\widetilde{\tau}} \equiv \partial u/\partial\widetilde{\tau}$ and the anomalous dimensions $\eta_{\phi/\chi} = -\partial_t \ln Z_{\phi/\chi}$. Furthermore, d is the spacetime dimension, $v_d^{-1} = 2^{d+1}\pi^{d/2}\Gamma(d/2)$ and d_γ is the dimension of the gamma matrices which is four in four spacetime dimensions. From here on, we suppress the tilde signs of the dimensionless couplings because from now on, we will only work with these. (2.65) is the equation of interest on which we apply various methods in order to find its fixed-point potentials. For this we need the flow equations of the couplings occurring in (2.65). For the anomalous dimensions η_ϕ and η_χ we use the equations derived in [29]. They read

$$\begin{aligned}\eta_\phi =& 8\frac{v_d}{d}\kappa\left\{2\lambda_1^2 m_{2,2}^d(0,2\kappa\lambda_1;\eta_\phi) + \frac{2N_\mathrm{f}^2-2}{4N_\mathrm{f}^2}\lambda_2^2 m_{2,2}^d\left(0,\frac{\kappa\lambda_2}{N_\mathrm{f}};\eta_\phi\right)\right\} + \\ & + 4 d_\gamma \frac{v_d}{d} N_\mathrm{c} h_\phi^2 m_4^{(F)d}\left(\frac{\kappa h_\phi^2}{N_\mathrm{f}};\eta_\chi\right),\end{aligned} \tag{2.66}$$

$$\begin{aligned}\eta_\chi =& \frac{4 v_d}{N_\mathrm{f} d} h_\phi^2\left\{N_\mathrm{f}^2 m_{1,2}^{(FB)d}\left(\frac{\kappa h_\phi^2}{N_\mathrm{f}},\bar{\varepsilon};\eta_\chi,\eta_\phi\right) + m_{1,2}^{(FB)d}\left(\frac{\kappa h_\phi^2}{N_\mathrm{f}},\bar{\varepsilon}+2\kappa\lambda_1;\eta_\chi,\eta_\phi\right) + \right. \\ & \left. + (N_\mathrm{f}^2-1) m_{1,2}^{(FB)d}\left(\frac{\kappa h_\phi^2}{N_\mathrm{f}},\bar{\varepsilon}+\frac{\kappa\lambda_2}{N_\mathrm{f}};\eta_\chi,\eta_\phi\right)\right\},\end{aligned} \tag{2.67}$$

with the dimensionless vacuum expectation value (VEV) $\kappa = Z_{\phi,k} k^{2-d}\rho_{0,k}$. Note that (2.67) corresponds to the expression for η_χ in Landau gauge where the gauge dependence cancels out. The flow equations for the gauge and Yukawa coupling are approximated in this work by their perturbative fixed-point values computed in [1] (2.34) and (2.35) which are expressed as expansions in $\epsilon = N_\mathrm{f}/N_\mathrm{c} - 11/2 \ll 1$. Furthermore, the flow equations for the lowest-order couplings can be derived from (2.65) through

$$\partial_t\bar{\varepsilon} = \partial_t u'\big|_{(\rho,\tau)=(0,0)}, \qquad \partial_t\lambda_1 = \partial_t u''\big|_{(\rho,\tau)=(0,0)}, \qquad \partial_t\lambda_2 = \partial_t u_{,\tau},\big|_{(\rho,\tau)=(0,0)}. \tag{2.68}$$

In the symmetric regime (upper case in (2.18)) and in the symmetry-breaking regime (lower case in (2.18)) we obtain the accompanying equations through

$$\partial_t \kappa = -\frac{1}{\lambda_1}\partial_t u'\Big|_{(\rho,\tau)=(\kappa,0)}, \qquad \partial_t \lambda_1 = \partial_t u''\big|_{(\rho,\tau)=(\kappa,0)}, \qquad \partial_t \lambda_2 = \partial_t u_{,\tau},\big|_{(\rho,\tau)=(\kappa,0)}. \tag{2.69}$$

In the symmetric regime they are of the form

$$\partial_t \bar{\varepsilon} = -(2-\eta_\phi)\bar{\varepsilon} - 2v_d\left\{\left[2({N_\mathrm{f}}^2+1)\lambda_1 + \frac{{N_\mathrm{f}}^2-1}{N_\mathrm{f}}\lambda_2\right] l_1^d(\bar{\varepsilon};\eta_\phi) - d_\gamma N_\mathrm{c} h_\phi^2 l_1^{(F)d}(0;\eta_\chi)\right\}, \tag{2.70}$$

$$\begin{aligned}\partial_t \lambda_1 =& (d-4+2\eta_\phi)\lambda_1 + 2v_d\left\{\left[2({N_\mathrm{f}}^2+4)\lambda_1^2 + \frac{{N_\mathrm{f}}^2-1}{N_\mathrm{f}}\lambda_2\left(2\lambda_1+\frac{\lambda_2}{N_\mathrm{f}}\right)\right] l_2^d(\bar{\varepsilon};\eta_\phi) + \right.\\ &\left. - d_\gamma \frac{N_\mathrm{c}}{N_\mathrm{f}} h_\phi^4 l_2^{(F)d}(0;\eta_\chi)\right\},\end{aligned} \tag{2.71}$$

$$\partial_t \lambda_2 = (d-4+2\eta_\phi)\lambda_2 + 2v_d\left\{\left[12\lambda_1\lambda_2 + \frac{2({N_\mathrm{f}}^2-3)}{N_\mathrm{f}}\lambda_2^2\right] l_2^d(\bar{\varepsilon};\eta_\phi) - 2d_\gamma N_\mathrm{c} h_\phi^4 l_2^{(F)d}(0;\eta_\chi)\right\}. \tag{2.72}$$

For the symmetry-breaking case they read

$$\begin{aligned}\partial_t \kappa =& (2-d-\eta_\phi)\kappa + 2v_d\left\{{N_\mathrm{f}}^2 l_1^2(0;\eta_\phi) + 3l_1^d(2\lambda_1\kappa;\eta_\phi)\right.\\ &\left. + ({N_\mathrm{f}}^2-1)\left(1+\frac{\lambda_2}{\lambda_1 N_\mathrm{f}}\right) l_1^d\left(\frac{\lambda_2\kappa}{N_\mathrm{f}};\eta_\phi\right) - d_\gamma N_\mathrm{c}\frac{h_\phi^2}{\lambda_1} l_1^{(F)d}\left(\frac{h_\phi^2\kappa}{N_\mathrm{f}};\eta_\chi\right)\right\},\end{aligned} \tag{2.73}$$

$$\begin{aligned}\partial_t \lambda_1 =& (d-4+2\eta_\phi)\lambda_1 + 2v_d\left\{{N_\mathrm{f}}^2\lambda_1^2 l_2^d(0;\eta_\phi) + 9\lambda_1^2 l_2^d(2\lambda_1\kappa;\eta_\phi)\right.\\ &\left. + ({N_\mathrm{f}}^2-1)\left(\lambda_1+\frac{\lambda_2}{N_\mathrm{f}}\right)^2 l_2^d\left(\frac{\lambda_2\kappa}{N_\mathrm{f}};\eta_\phi\right) - d_\gamma\frac{N_\mathrm{c}}{N_\mathrm{f}} h_\phi^4 l_2^{(F)d}\left(\frac{h_\phi^2\kappa}{N_\mathrm{f}};\eta_\chi\right)\right\},\end{aligned} \tag{2.74}$$

$$\begin{aligned}\partial_t \lambda_2 =& (d-4+2\eta_\phi)\lambda_2 + 2v_d\left\{\frac{N_\mathrm{f}}{4}\lambda_2^2 l_2^d(0;\eta_\phi) + \frac{9({N_\mathrm{f}}^2-4)}{4N_\mathrm{f}}\lambda_2^2 l_2^d\left(\frac{\lambda_2\kappa}{N_\mathrm{f}};\eta_\phi\right) - \frac{N_\mathrm{f}}{2}\lambda_2^2 l_{1,1}^d\left(0,\frac{\lambda_2\kappa}{N_\mathrm{f}};\eta_\phi\right)\right.\\ &\left. + 3\left(\frac{\lambda_2}{N_\mathrm{f}}+4\lambda_1\right)\lambda_2 l_{1,1}^d\left(2\lambda_1\kappa,\frac{\lambda_2\kappa}{N_\mathrm{f}};\eta_\phi\right) - 2d_\gamma N_\mathrm{c} h_\phi^4 l_2^{(F)d}\left(\frac{h_\phi^2\kappa}{N_\mathrm{f}};\eta_\chi\right)\right\}.\end{aligned} \tag{2.75}$$

The equations (2.70)-(2.75) which we have obtained from (2.65) are in accordance with the results from [29]. Equipped with this set of equations, we are finally in the position to compute the fixed-point potential. The methods used for this purpose are explained in chapter 3.

2.3.3. Deep Euclidean region of FRG equations

Let us as a final section of this chapter compare the perturbative calculations of [1] summarized in section 2.3.1 with FRG results of section 2.3.2 in the deep Euclidean region ($k^2 \gg m^2$ such that masses can be neglected). We start with the equations for the anomalous dimensions (2.66) and (2.67). Setting $\bar{\varepsilon} = \kappa = 0$ and $\eta_\phi = \eta_\chi = 0$ (neglecting higher loop corrections) in the threshold functions, we obtain the perturbative equations in the deep Euclidean region as

$$\eta_\phi = \frac{N_\mathrm{c}}{8\pi^2} h_\phi^2, \qquad \eta_\chi = \frac{N_\mathrm{f}}{16\pi^2} h_\phi^2. \tag{2.76}$$

The same computations can be done for the couplings λ_1 and λ_2:

$$\partial_t \lambda_2 = -\frac{N_\mathrm{c}}{2\pi^2} h_\phi^4 + \frac{N_\mathrm{c}}{4\pi^2} h_\phi^2 \lambda_2 + \frac{3}{4\pi^2} \lambda_1 \lambda_2 + \frac{{N_\mathrm{f}}^2 - 3}{8\pi^2 N_\mathrm{f}} \lambda_2^2, \tag{2.77}$$

$$\partial_t \lambda_1 = -\frac{N_\mathrm{c}}{4\pi^2 N_\mathrm{f}} h_\phi^4 + \frac{N_\mathrm{c}}{4\pi^2} h_\phi^2 \lambda_1 + \frac{{N_\mathrm{f}}^2 + 4}{8\pi^2} \lambda_1^2 + \frac{{N_\mathrm{f}}^2 - 1}{16\pi^2 {N_\mathrm{f}}^2} \lambda_2^2 + \frac{{N_\mathrm{f}}^2 - 1}{8\pi^2 N_\mathrm{f}} \lambda_1 \lambda_2. \tag{2.78}$$

This can be compared with the perturbative calculations (2.26) and (2.27) rewritten in our nomenclature using (2.19) in terms of λ_1 and λ_2:

$$\partial_t \lambda_2 = -\frac{N_\mathrm{c}}{2\pi^2} h_\phi^4 + \frac{N_\mathrm{c}}{4\pi^2} h_\phi^2 \lambda_2 + \frac{N_\mathrm{f}}{8\pi^2} \lambda_2^2, \tag{2.79}$$

$$\partial_t \lambda_1 = -\frac{N_\mathrm{c}}{4\pi^2 N_\mathrm{f}} h_\phi^4 + \frac{N_\mathrm{c}}{4\pi^2} h_\phi^2 \lambda_1 + \frac{{N_\mathrm{f}}^2}{8\pi^2} \lambda_1^2 + \frac{1}{16\pi^2} \lambda_2^2 + \frac{N_\mathrm{f}}{8\pi^2} \lambda_1 \lambda_2, \tag{2.80}$$

where we see differences to (2.77) and (2.78) in the scalar sector. Those differences decrease with decreasing ϵ (increasing N_f). Thus, both equations agree in the large N_f limit.

3. Methods to solve fixed-point equations and a benchmark test

In general, fixed-point equations are partial differential equations of second order. In our case they can be simplified to ordinary differential equations (ODEs) using simpler truncations in the effective average action. The space of solutions of such ODEs is parametrized by two initial conditions since they are of second order. Moreover, fixed-point equations typically have movable singularities. Those singularities are movable singular points since their location depends on the initial condition of the underlying differential equation. Effects of such singularities can be explained best using a simple example, the Wilson-Fisher fixed-point potential of the Ising model below $d < 4$ (also called $\mathcal{O}(1)$ model). This model will also serve as a benchmark test which makes it worth introducing here. The ansatz for the effective average action reads

$$\Gamma_k[\varphi] = \int \mathrm{d}^d x \left[\frac{1}{2} Z_k(\varphi^2) \partial_\mu \varphi \partial^\mu \varphi + V_k(\varphi^2) \right]. \tag{3.1}$$

Setting the wave function renormalization $Z_k(\varphi^2) \equiv 1$ yields in the so-called local potential approximation (LPA). Thus, the anomalous dimension η_ϕ is zero. From here, we can deduce the fixed-point equation using the machinery explained in section 2.3.2. In dimensionless form, it results in (see for instance [32])

$$0 = -d\,v + \frac{d-2}{2}\varphi\, v'(\varphi) + \frac{4 v_d}{d} \frac{1}{1 + v''(\varphi)}, \tag{3.2}$$

for the $\mathbb{Z}_2$-invariant potential $v(\varphi)$ with the order parameter φ. For the purpose of movable singularities[1] it is convenient to rewrite (3.2) as

$$v'' = -\frac{4 v_d}{d} \frac{e(v, v'; \varphi)}{s(v, v'; \varphi)}, \qquad s(v, v'; \varphi) = -d\,v + \frac{d-2}{d}\varphi\, v', \qquad e(v, v'; \varphi) = 1 + \frac{d\, s(v, v'; \varphi)}{4 v_d}. \tag{3.3}$$

At this point, we can investigate the effects of the movable singularity on the space of solutions. At first, the $\mathbb{Z}_2$ symmetry requires $v'(\varphi = 0) = 0$, reducing the solution space to one parameter which could for instance be $\sigma := v''(\varphi = 0)$. Moreover, if we have a closer look at (3.3), we see that integrating the ODE from $\varphi = 0$ to larger field amplitudes, $s(v, v'; \varphi)$ exhibits a zero when the two terms cancel. This indicates the movable singularity whose location depends on σ. Nevertheless, a global solution can exist if $e(v, v'; \varphi)$ vanishes sufficiently fast at the same field value. This condition quantizes the one parameter space of solutions. In the case of the Ising model only one non-trivial and globally defined fixed-point potential remains, the well known Wilson-Fisher fixed-point potential. This idea generalizes two more complex ODEs like the one for the Gauge-Yukawa class.

[1] The following part follows the line of reasoning in [32].

3.1. Methods

From this simple example we have seen how movable singularities shrink the space of possible solutions of fixed-point potentials. In order to find global solutions (or in other words a particular value of σ) we need to introduce methods which can handle such singularities. The following section is devoted to these methods which will be used later on to first recover known results of the $\mathcal{O}(1)$ model and the Gross-Neveu model and then to find global solutions of the Gauge-Yukawa theories. We first introduce the small- and large-field expansion and the shooting method which are well established from statistical physics and conclude with a pseudo-spectral method which has broad applications as well in fluid dynamics or general relativity.

3.1.1. Small-field expansion

A first approximate analytical method to solve an ODE for small-field values ρ is the small-field expansion (SFE). Here we expand the fixed-point potential u^* around $\rho = 0$ as a power series

$$u^*(\rho) = \sum_{i=0}^{N_{\text{trunc}}} \frac{c_i}{i!} \rho^i, \tag{3.4}$$

up to a truncation order N_{trunc} with $\rho = \text{Tr}\,\phi^2/2$ such that the potential preserves $\mathbb{Z}_2$ symmetry. This ansatz is only valid in the domain $0 \leq \rho \leq \rho_s < \infty$ for two reasons. We expand around small fields up to a finite order and for large field values the potential needs to fulfill its asymptotic behavior given by the dimensional part of the flow equation. This is not the case if (3.4) would be valid for arbitrary large fields. Inserting the ansatz (3.4) into a fixed-point equation yields

$$0 \stackrel{!}{=} \partial_t u^*(\rho) = \sum_{i=0}^{N_{\text{trunc}}} \beta_i(\{c_n\}) \rho^i, \tag{3.5}$$

where we find the β functions introduced in section 2.2 as

$$\beta_i(\{c_n\}) = \partial_t c_i = \partial_t \left(\left(\partial_\rho\right)^i u(\rho) \Big|_{\rho=0} \right). \tag{3.6}$$

Each β_n depends on all couplings $c_0,..,c_{n+1}$ and, of course, vanishes at the fixed point. Thus, there is manifestly one free parameter which we choose to be the mass term $c_1 := \lambda$ and all other couplings can be written in terms of λ (which can be done by solving the coupled system of algebraic equations). This mass term needs to be fine-tuned such that it fulfills the requirements concerning the movable singularity explained above. There are now two ways in which this can be done. The first, straightforward way as e.g. done in [16, 17] is to set $\beta_{N_{\text{trunc}}} = P_{N_{\text{trunc-1}}}(\lambda^*) = 0$ where $P_{N_{\text{trunc-1}}}(\lambda^*)$ is a polynomial of order $N_{\text{trunc}} - 1$ which exhibits several roots λ^*. We choose all roots which converge for large N_{trunc} to fixed values. This choice ensures that the approximating polynomials converge to a power series with maximal radius of convergence (such that the power series is valid up to the field value ρ_s). The second, numerically less expensive way of fine-tuning λ, or in other words, finding the maximal radius of convergence is to compare the quotients of successive couplings, namely c_n/c_{n+1} for large n [33][2]. Roughly speaking, c_n/c_{n+1} increases with increasing radius of convergence since the couplings decrease faster with increasing order. In practice, we set λ to value in $(-1, 1)$ with some step size and look for the specific values λ^* where c_n/c_{n+1} exhibits a maximum for different values of n. Those λ^* are the possible

[2] Notice that the quotient reminds of the inverse of the ratio test where one can find out if a power series is convergent ($|a_{n+1}/a_n| = q < 1$). It as well serves as a method to compute the radius of convergence of the series which makes it usable for our purposes. The radius of convergence is given by $1/q$.

values for the global potential.
All those calculations can as well be done with a slightly different ansatz for u^* if the potential has a non-trivial minimum κ. Then it could be advantageous to expand the potential as

$$u^*_{\mathrm{SB}}(\rho-\kappa) = \tilde{c}_0 + \frac{\lambda_1}{2}(\rho-\kappa)^2 + \sum_{i=3}^{N_{\mathrm{trunc}}} \tilde{c}_i(\rho-\kappa)^i\,, \tag{3.7}$$

because the convergence properties are in general better if the potential is symmetry breaking. Here, κ takes over the tasks of λ in the symmetric case and the initial conditions are adapted:

$$u'(\rho=\kappa)=0, \qquad u''(\rho=\kappa)=\sigma. \tag{3.8}$$

3.1.2. Large-field expansion

We have seen in section 3.1.1 that we are, until now, only able to construct the potential up to a field value ρ_s. Since flow equations are nonperturbative they apply to arbitrarily large field values (the potential shows an asymptotic behavior of the form $u \propto \rho^{\frac{d}{d-2+\eta_\phi}} = \rho^{N_\infty}$). Hence, we can expand the potential as a power series around this asymptotic behavior for large field values. This expansion is called large-field expansion (LFE). For some ODEs like (3.2) the ansatz

$$u^*_L(\rho) = \xi_\infty \rho^{N_\infty} + \sum_{n=0}^{N_{\mathrm{trunc}}} \xi_{-n}\rho^{-n} \tag{3.9}$$

is satisfactory. For the Gauge-Yukawa class (2.13) the ansatz

$$u^*_L(\rho) = A\rho^{N_\infty} + \sum_{i=1}^{N_{\mathrm{trunc}}} c_{L,i}\rho^{i(1-N_\infty)} + \sum_{i=0}^{\widetilde{N}_{\mathrm{trunc}}} \gamma_{L,i}\rho^{-i} \tag{3.10}$$

is more useful as suggested in [32]. Computing the constants ξ_{-n}, $c_{L,i}$ and $\gamma_{L,i}$ as a function of the free parameter ξ_∞ (or A) in the same fashion as above, we aim at the fixed-point potential on the interval $[\rho_A,\infty)$. The free parameter A is then chosen in such a way that we glue the small- and large-field expansions together "in the best possible way" at some point ρ^* which should satisfy

$$\rho_A \le \rho^* \le \rho_s. \tag{3.11}$$

This means, the power series have overlapping radii of convergence and an interval where both expansions are valid. The "best possible way" could for instance be to minimize the error between the solutions in an interval where both are valid [18]. If this is the case, we have constructed a global fixed-point potential.

3.1.3. Shooting from the origin

A well-tested method e.g. [32, 34–36] for many FRG equations is the numerical shooting. The general procedure is the following: We take two initial conditions (we have ODEs of second order) which could be $u'(\rho=0)=\lambda$ and $u''(\rho=0)=\sigma$. Using those conditions, we can numerically integrate out from the origin $\rho=0$ until we hit the movable singularity. Varying again λ in $(-1,1)$ we can find λ^* which is the point ρ_s where the radius of convergence is maximal such that we can construct the fixed-point potential up to ρ_s.

3.1.4. Pseudo-spectral method

Pseudo-spectral methods (PSM) are heavily used in different disciplines in physics like fluid dynamics [37] or general relativity [22] and were first applied to FRG problems by [21,23,38]. These applications were improved by [19] in particular concerning global solutions using a new ansatz for large fields. In the following we will explain this improved method invented in [19].
For a construction of a global solution of FRG equations, the pseudo-spectral method uses Chebyshev polynomials of the first kind, which are defined by

$$T_n(\cos(x)) = \cos(nx), \qquad n \in \mathbb{N}_0, \tag{3.12}$$

and rational Chebyshev polynomials of the first kind

$$R_n(x) = T_n\left(\frac{x-L}{x+L}\right), \tag{3.13}$$

with a compactification parameter $L > 0$. PSM use Chebyshev polynomials since flow equations have a fixed asymptotic behavior which should as well be fixed by the approximation scheme independent of the interpolation order. This property is fulfilled by the rational Chebyshev polynomials (3.13). Furthermore, the coefficients of the (rational) Chebyshev polynomials have an exceptional convergence (since they are related to Fourier series). For example, a Chebyshev expansion of a Lipschitz continuous function always converges exponentially. One can see that in a log-log-plot of the coefficients over the order. Exponential convergence is indicated by a convex curve and algebraic convergence by a straight line.
Let us name some more important properties (proofs can be found e.g. in [39]) of the Chebychev polynomials which are used frequently in our implementation of the method. First, the polynomials fulfill the recurrence relation

$$T_{n+1}(x) = 2xT_n(x) - T_{n-1}(x) \tag{3.14}$$

with which a smooth function $f(x)$ on $[-1,1]$ expanded in Chebyshev polynomials

$$f(x) = \sum_{i=0}^{N} a_i T_i(x) \tag{3.15}$$

can be evaluated quickly and numerically stable using the Clenshaw algorithm (following from (3.14)):

$$b_{N+2} = b_{N+1} = 0, \qquad b_i = a_i + 2xb_{i+1} - b_{i+2}, \qquad f(x) = a_0 + xb_1 - b_2. \tag{3.16}$$

The derivative of $f(x)$ expanded as a sum of Chebyshev polynomials of order $N-1$ with coefficients a'_i is given recursively by

$$a'_{N-1} = 2Na_N, \qquad a'_{N-2} = 2(N-1)a_{N-1}, \qquad a'_i = 2(i+1)a_{i+1} + a'_{i+2}. \tag{3.17}$$

Since the Chebyshev polynomials are only defined on the interval $[-1,1]$ and we want to solve flow equations on $[0,\infty)$ we need affine transformations to map intervals of $[0,\infty)$ to $[-1,1]$. First, we can, for instance, map some $x \in [a,b]$ with a,b finite to $x' \in [-1,1]$ by

$$x \longmapsto x' = \frac{2}{b-a}x - \frac{a+b}{b-a} \tag{3.18}$$

with the inverse transformation

$$x' \longmapsto x = \frac{a+b}{2} + \frac{b-a}{2}x'. \tag{3.19}$$

Further, we can as well find a transformation that maps $x \in [x_0, \infty]$ to $x' \in [-1, 1]$:

$$x \longmapsto x' = \frac{x - x_0 - L}{x - x_0 + L}, \tag{3.20}$$

and its inverse transformation

$$x' \longmapsto x = \frac{x'(x_0 - L) - x_0 - L}{x' - 1}. \tag{3.21}$$

Now we can set the stage for the implementation of the PSM. Assume an ODE restricted to the domain $\mathbb{R}_+$ of the form

$$\mathcal{L}[f(x)] = 0, \tag{3.22}$$

which we want to solve using Chebyshev polynomials with a (non-)linear integro-differential operator $\mathcal{L}$. To do so, we decompose the domain $\mathbb{R}_+$ into M parts and expand $f(x)$ into a series of Chebyshev polynomials on each part. The higher the number of decomposed parts, the better and faster is the convergence of the coefficients. Restricting to $M = 2$ parts (resulting in a decomposition of the form $[0, x_0]$ and $[x_0, \infty]$) we expand $f(x)$ as

$$f(x) = \begin{cases} \sum_{i=0}^{N_c} c_i T_i\left(\frac{2x}{x0} - 1\right), & x \in [0, x_0] \\ f_\infty(x) \sum_{i=0}^{N_r} r_i R_i(x - x_0), & x \in [x_0, \infty). \end{cases} \tag{3.23}$$

In $[0, x_0]$ we expand $f(x)$ with the standard Chebyshev polynomials with c_i the Chebyshev coefficients whereas in $x \in [x_0, \infty)$ we use a rational Chebyshev series with expansion coefficients r_i. Here $f_\infty(x)$ represents the asymptotic behavior (given by the dimensional scaling properties of the FRG equation) of the solutions which is easily calculable in many cases. Inserting (3.23) into (3.22) the Chebyshev coefficients can be determined via the collocation method. It evaluates the equation at a certain number of collocation points depending on the order of the expansion such that a system of algebraic equations arises. This system can e.g. be solved by a Newton-Raphson method. It turns out that the best choice for a high accuracy is choosing the collocation points x_k to be

$$x_k = \cos\left(\frac{2k - 1}{2n}\pi\right), \qquad k = 1, ..., n, \tag{3.24}$$

the nodes of the Chebyshev polynomials T_n(another equivalent choice would be the extrema of T_n). Since we split up the domain in different parts, the solutions need to be matched together smoothly. To achieve this $p - 1$ derivatives need to be matched at the intermediate point(s) for a differential equation of order p. In the case $M = 2$ the matching point would be x_0. The number of collocation points then depends on the order of the series expansion and on the number of matching conditions. Moreover, (3.23) has two free parameters, namely x_0 and the compactification parameter L. x_0 needs to be chosen such that it includes the essential physics, for example the vacuum expectation value, whereas L can be chosen freely because the rational expansion essentially interpolates the asymptotic expansion. The influence of L is therefore small. This scheme can easily be generalized to $M > 2$.

3.2. A benchmark test

The $O(1)$- or Ising model serves as a good model for testing the implementation of the methods described above since it is a well-studied, simple system (e.g. [16, 17, 19, 21]) which exhibits a non-Gaussian fixed point. We have described it already at the beginning of chapter 3. The fixed-point equation in the LPA we aim to solve is (3.2) in $d = 3$ dimensions where we introduce $\rho = \varphi^2/2$. It reads

$$0 = -3v + \rho v'(\rho) + \frac{1}{6\pi^2}\frac{1}{1 + v' + 2\rho v''(\rho)},$$

where the prime denotes now the derivative with respect to ρ. Using the small-field expansion we obtain a system of algebraic equations of the form (3.6) where we set each β function to zero since we are interested in the fixed points. Solving this system, we find the first few couplings c_i depending on λ $(= c_1)$ as

$$\begin{aligned} c_0 &= \frac{1}{18\pi^2(1+\lambda)}, & c_1 &= \lambda, \\ c_2 &= -4\pi^2\lambda(1+\lambda)^2, & c_3 &= -\frac{72}{15}\pi^4\lambda(1+\lambda)^3(1+13\lambda), \\ c_4 &= -\frac{1728}{7}\pi^6\lambda^2(1+\lambda)^4(1+7\lambda), & c_5 &= \frac{768}{7}\pi^8\lambda^2(1+\lambda)^5(2+121\lambda+623\lambda^2), \end{aligned} \tag{3.25}$$

which can be continued arbitrarily far. As described in 3.1.1 we now set each c_i to zero, solve for λ and look for roots which occur in each equation. We can picture all roots in $(-1, 1)$ in

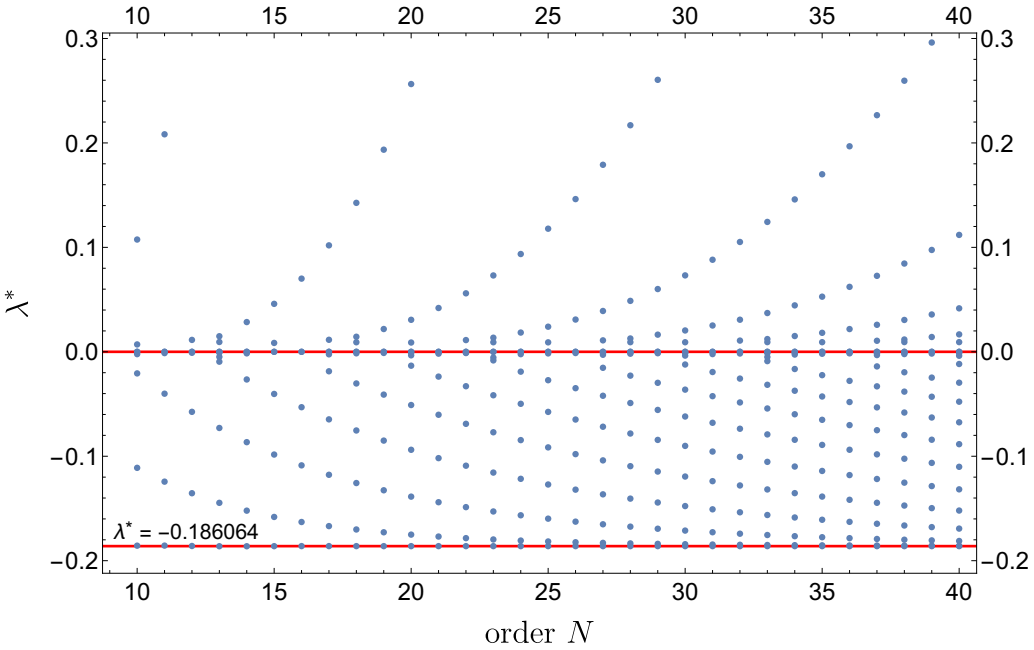

Figure 3.1.: Roots for λ of c_i up to order $i = 40$. We see a Gaussian fixed point at $\lambda^* = 0$ and an interacting fixed point located at $\lambda^* = -0.186064$.

figure 3.1 where we see a Gaussian fixed point occurring at $\lambda^* = 0$ and the interacting fixed point at $\lambda^* = -0.186064$ which is an accordance with e.g. [16]. This is the case since all roots $\lambda > 0$ do not converge to a fixed value whereas every root $\lambda < 0$ converges against the fixed-point

value $\lambda^* = -0.186064$. Inserting λ^* into the set of algebraic equations (3.25) results in the fixed-point potential (3.4) for small fields up to arbitrarily high order in the expansion series. In the next step we approximate the solution for large field values using the large-field expansion. The asymptotic behavior of (3.2) is found to be $v \propto \varphi^3$. Proceeding the same way as above we find the fixed-point potential depending on the free parameter A

$$v_L(\rho) = A\rho^3 + \frac{1}{450\pi^2 A\rho^2} - \frac{1}{9450\pi^2 A^2\rho^4} + \frac{1}{182250\pi^2 A^3\rho^6} + \cdots . \tag{3.26}$$

We observe that the radii of convergence of both series overlap[3]. Thus, both solutions can be glued together in some interval of the overlap region (ρ_L, ρ_S) where $\rho_{S,L}$ is the radius of convergence of the small-/large-field expansion. The gluing is now done in such a way that the error in the overlap region between both expansions gets minimized:

$$0 \stackrel{!}{=} \frac{\mathrm{d}}{\mathrm{d}A} \int_{\rho_L}^{\rho_S} \mathrm{d}\rho \left(v_L(\rho) - v_S(\rho)\right)^2 \tag{3.27}$$

Hence, A is fixed by this condition and we are left with a global fixed-point potential. For the $O(1)$-model we set $\rho_L = 0.08$ and $\rho_S = 0.1$ (which could be chosen differently) with the result $A \approx 28.60926$ which is in accordance with [18]. Graphically, the solution is given in 3.2. We see

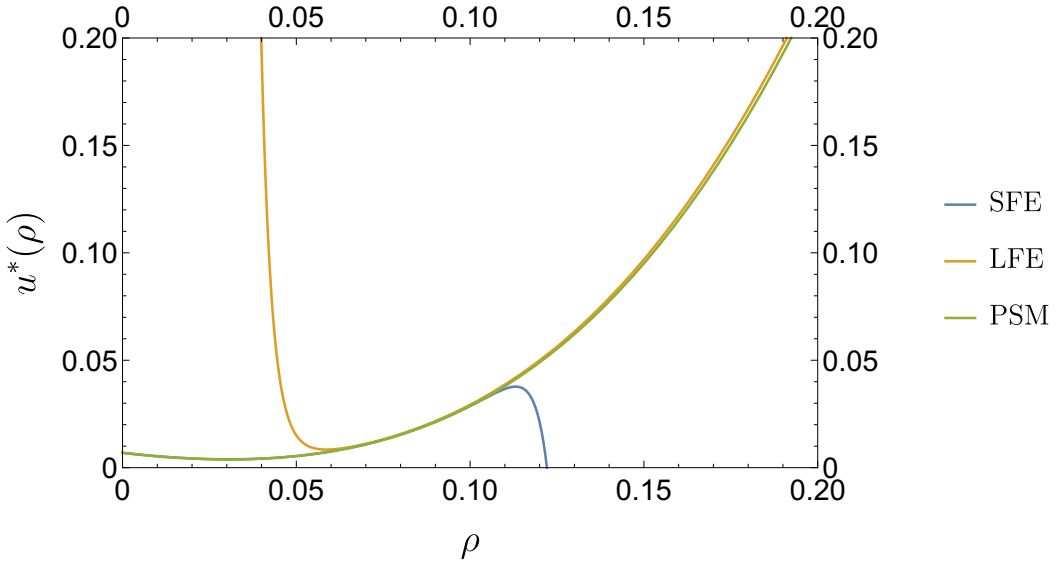

Figure 3.2.: Fixed-point potential constructed with the small-field expansion (blue), the large-field expansion (yellow) and the pseudo-spectral method (green). The overlap region of the small- and large-field expansions can be seen clearly.

that the small-field expansion (blue curve) indeed is just valid up to $\rho \approx 0.1$ whereas the large-field expansion (yellow curve) is valid from $\rho \approx 0.06$, resulting in an overlap region.

[3] This can most easily be seen graphically in figure 3.2.

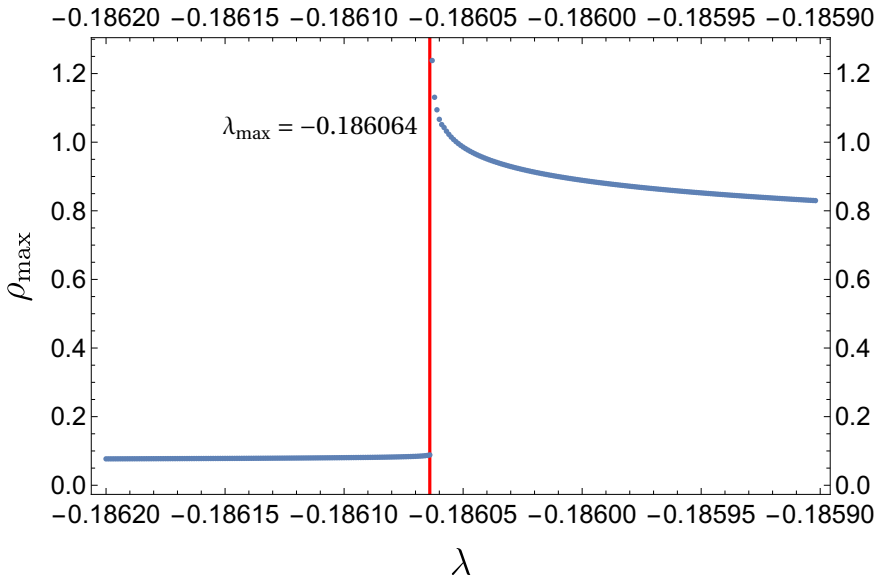

Figure 3.3.: Position of the movable singularity $\rho_{\max}$ plotted for different values of the mass λ. The value $\lambda_{\max} = -0.186064$ is the point where the radius of convergence is maximized since the singularity is the most far away from the origin and thus $\lambda_{\max}$ is the fixed-point value of the system.

Another possibility to find the fixed-point value λ^* is the numerical shooting (see section 3.1.3). With this method we can confirm the results from above. We find again $\lambda^* = -0.186064$ for the Wilson-Fisher fixed point. This is illustrated in figure 3.3.

At last, we want to test the implementation of the pseudo-spectral method. The crucial point here is to solve the algebraic set of equations (originated from the collocation points and the matching conditions). This is done iteratively and numerically with the Newton-Raphson method. To obtain a true solution of the set of equations we need to start with a good initial guess to make sure the solver runs into the true minimum and not into a numerical artifact. Therefore we can use the solutions we have gained from the small- and large-field expansions[4]. The solution is as well shown in figure 3.2 in green. We have chosen the number of parts $M = 2$, the matching point $x_0 = 0.3$ and the compactification parameter $L = 1$ as suggested by [19]. We see that the PSM gives a global solution right away with better convergence properties and confirms the solution from before.
In the course of this work the same methods have additionally been tested within the partially bosonized Gross-Neveu model with

$$\Gamma_k\left[\overline{\psi},\psi,\phi\right] = \int_x \left[\frac{N_\mathrm{f}}{2} Z_{\phi,k}(\partial_\mu\phi)^2 + \overline{\psi}(Z_{\psi,k}\,\mathrm{i}\partial\!\!\!/ + \mathrm{i}\,h_{\phi,k}\phi)\psi + N_\mathrm{f} U_k(\phi^2)\right] \tag{3.28}$$

as an ansatz for the effective average action [20]. Here, the anomalous dimensions and the Yukawa coupling were encountered as well such that a system of equations needs to be solved. Doing that, we were able to confirm the results of [20] where this model is computed in detail. We conclude from these two examples that the implemented methods work properly and that we can start applying them onto the more complex model of Gauge-Yukawa theories where we

[4] More detailed information regarding the implementation of the PSM is given in section 4.2.2.

cannot compare the results of global fixed-point potentials with the literature (apart from the perturbative results by [1]).

4. Global fixed-point potentials of the Gauge-Yukawa class

In this chapter we discuss the fixed-point landscape of the scalar sector of the Gauge-Yukawa class described by the Lagrangian (2.16). To recap, in Euclidean space it reads

$$\mathcal{L} \equiv \mathcal{L}_E = \frac{1}{2}\operatorname{Tr} F^{\mu\nu}F_{\mu\nu} + \bar{\chi}^i i\not{D}\chi^i + i h_\phi \bar{\chi}^i \phi^{ij}\chi^j + \frac{1}{2}\left(\partial_\mu \phi^{ij}\partial^\mu \phi^{ji}\right) + U(\phi^2), \tag{4.1}$$

with its resulting flow equations written down in section 2.3. The equation of interest is the flow equation for the scalar potential (2.65) because it describes the fixed points in the scalar sector. It is given by

$$\begin{aligned}\partial_t u = &-d\,u + (d-2+\eta_\phi)\rho\,u' + (2d-4+2\eta_\phi)\tau\,u_{,\tau} + \frac{4v_d}{d}\left(1-\frac{\eta_\phi}{d+2}\right)\sum_{i=1}^{2N_{\mathrm{f}}{}^2}\frac{1}{1+\mathfrak{m}_i^2} + \\ &-\frac{4v_d}{d}\,d_\gamma N_{\mathrm{c}}\left(1-\frac{\eta_\chi}{d+1}\right)\left[\frac{N_{\mathrm{f}}-1}{1+m^2h_\phi^2} + \frac{1}{1+m^2\varepsilon^2 h_\phi^2}\right].\end{aligned} \tag{4.2}$$

In order to solve (4.2) we use the flow equations for the anomalous dimensions (2.66) and (2.67) (symmetric regime[1]) together with the perturbative result for the Yukawa coupling (2.34) at their corresponding fixed points. (4.2) is a partial differential equation which is truncated in the potential since it includes only two of the N_{f} invariants, namely ρ and τ, up to finite order. In the following we specify our calculations to the ρ direction but we want to keep the influence of the coupling λ_2 belonging to the τ direction for two reasons. First, it simplifies (4.2) enormously because we obtain an ordinary differential equation on which we can apply the methods of chapter 3. The second reason why we specify to the ρ direction is that it is the important direction for giving all fermions a mass. Mathematically, this means that we set τ to zero but keep λ_2 as a small

Table 4.1.: Simplified scalar mass spectrum by setting $\tau = 0$ but keeping λ_2 as a small parameter.

Eigenvalue $\mathfrak{m}_i^2$	Degeneracy
$u' + \frac{\rho\lambda_2}{N_{\mathrm{f}}}$	$N_{\mathrm{f}}{}^2 - 1$
u'	$N_{\mathrm{f}}{}^2$
$u' + 2\rho u''$	1

parameter. Hence, the real parameters which have been used to parameterize the subspace of scalar configurations simplify such that $\varepsilon^2 = 1$ and $m^2 = \rho/N_{\mathrm{f}}$. The resulting scalar mass spectrum is shown in table 4.1 with only three different eigenvalues left. Starting from the general

[1] Note that we use the symmetric equations for simplicity. The advantage is, that the anomalous dimensions can then be solved separately. This approximation is satisfactory since $\eta_i \ll d$, $i = \phi, \chi$ as we will see in section 4.2.3.

flow equation for the scalar potential (2.65) we can plug in the results from above, ending up with

$$\begin{aligned}\partial_t u =& -d\,u + (d-2+\eta_\phi)\rho u' + \frac{4v_d}{d}\left(1-\frac{\eta_\phi}{d+2}\right)\left[\frac{{N_\mathrm{f}}^2-1}{1+u'+\frac{\rho\lambda_2}{N_\mathrm{f}}} + \frac{{N_\mathrm{f}}^2}{1+u'} + \frac{1}{1+u'+2\rho u''}\right] + \\ &- \frac{4v_d}{d} d_\gamma N_\mathrm{c} N_\mathrm{f}\left(1-\frac{\eta_\psi}{d+1}\right)\frac{1}{1+\frac{\rho}{N_\mathrm{f}}h_\phi^2},\end{aligned} \tag{4.3}$$

where one ingredient, namely the flow equation for λ_2 still has to be specified, to be able to apply the introduced methods onto (4.3). Therefore we use its flow equation (2.72) in the symmetric regime where we take the results of appendix B to evaluate the threshold function analytically. We obtain

$$\partial_t \lambda_2 = (d-4+2\eta_\phi)\lambda_2 + 2v_d\left(1-\frac{\eta_\phi}{d+2}\right)\frac{1}{(1+\bar{\varepsilon})^3}\left(12\lambda_1\lambda_2 + \frac{2({N_\mathrm{f}}^2-3)}{N_\mathrm{f}}\lambda_2^2\right) - \frac{N_\mathrm{c}}{2\pi^2}h_\phi^4\left(1-\frac{\eta_\chi}{d+1}\right). \tag{4.4}$$

This equation can be solved for λ_2 at the fixed point $\partial_t\lambda_2 = 0$ such that we get λ_2^* as a function of the other couplings which can be inserted into the fixed-point equation for the scalar potential. Since the equation is quadratically, we find two solutions for λ_2^* as it is the case perturbatively. Analogously to [1], it will turn out that only the bigger solutions exhibits fixed points. Finally, the stage is now set for the calculation.

4.1. Fixed-point landscape for general N_f

Summarizing the above recipe for the fixed-point calculation, we are left with a system of coupled equations, where three of them are of algebraic nature (4.5)-(4.7) and (4.8) is an ODE:

$$\begin{aligned}0 =& (d-4+2\eta_\phi)\lambda_2 + 2v_d\left(1-\frac{\eta_\phi}{d+2}\right)\frac{1}{(1+\bar{\varepsilon})^3}\left(12\lambda_1\lambda_2 + \frac{2({N_\mathrm{f}}^2-3)}{N_\mathrm{f}}\lambda_2^2\right) + \\ &- \frac{N_\mathrm{c}}{2\pi^2}h_\phi^4\left(1-\frac{\eta_\chi}{d+1}\right),\end{aligned} \tag{4.5}$$

$$\eta_\phi = \frac{4v_d}{d} d_\gamma N_\mathrm{c} h_\phi^2\left(1+\frac{1-\eta_\chi}{d-2} - \frac{1-\eta_\chi}{2d-4} - \frac{1}{4}\right), \tag{4.6}$$

$$\eta_\chi = \frac{8v_d}{d} N_\mathrm{f}\left(1-\frac{\eta_\phi}{d+1}\right)\frac{1}{(1+\bar{\varepsilon})^2}, \tag{4.7}$$

$$\begin{aligned}0 =& -d\,u + (d-2+\eta_\phi)\rho u' + \frac{4v_d}{d}\left(1-\frac{\eta_\phi}{d+2}\right)\left[\frac{{N_\mathrm{f}}^2-1}{1+u'+\frac{\rho\lambda_2}{N_\mathrm{f}}} + \frac{{N_\mathrm{f}}^2}{1+u'} + \frac{1}{1+u'+2\rho u''}\right] + \\ &- \frac{4v_d}{d} d_\gamma N_\mathrm{c} N_\mathrm{f}\left(1-\frac{\eta_\psi}{d+1}\right)\frac{1}{1+\frac{\rho}{N_\mathrm{f}}h_\phi^2}.\end{aligned} \tag{4.8}$$

This system exhibits two fixed points if we choose the bigger solution for λ_2^* of (4.5), independently of N_f and N_c. If the smaller solution of λ_2^* is chosen, no fixed points are obtained. Thus, we will not consider the smaller solution any more. One of the fixed points results in a symmetry-breaking fixed-point potential and one in a "locally symmetric" potential[2]. We will find in the following that those two are equivalent to the fixed points found by Litim and Sannino in [1] which were described in section 2.3.1. We have called them there $(\alpha_g^*, \alpha_y^*, \alpha_{h1}^*, \alpha_{v1}^*)$ (symmetry-breaking potential) and $(\alpha_g^*, \alpha_y^*, \alpha_{h1}^*, \alpha_{v2}^*)$ (locally symmetric potential). In the course of this

[2] We do not speak here of a symmetric potential since it is not entirely true due to non-trivial extrema of the fixed-point potential. This can be seen in figure 4.2 (b).

chapter those two fixed points will be investigated in detail. To do so, we proceed as follows. We start with the small-field expansion where we find all possible fixed points and compute the corresponding large-field expansion. Afterwards, the system (4.5)-(4.8) will be investigated with the help of the shooting method to get a better estimate of the radius of convergence. At last, we construct the potentials at the fixed points globally with the PSM. We focus on the special configuration $N_f = 28$ and $N_c = 5$ ($\epsilon = 0.1$) first where we do the analysis in detail but we will as well briefly summarize results for smaller values of ϵ later in section 4.3. There are two reasons to consider the smallest (N_c, N_f) configuration in detail: The small numbers are easier to handle numerically (especially for the PSM) and the perturbative results are most inaccurate for this configuration because it is the one with the largest ϵ.

4.2. The $N_f = 28$ and $N_c = 5$ configuration

4.2.1. First attempts at constructing fixed-point potentials

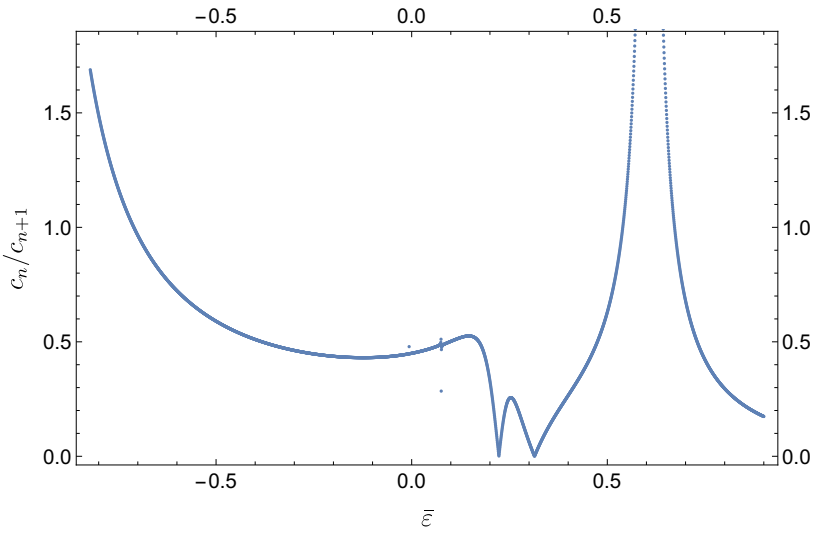

Figure 4.1.: The ratio c_n/c_{n+1} plotted for $N_f = 28$, $N_c = 5$ at order $n = 14$ over the mass coupling $\bar{\varepsilon}$. $\bar{\varepsilon}$ is fine-tuned in the interval $(-1, 1)$. In this plot we find the local maxima which could be fixed points located at $\bar{\varepsilon}^* \in \{-0.0065, 0.0754, 0.1465, 0.2535, 0.608\}$.

When plugging in specific numbers for N_f and N_c, we are able to determine the fixed-point values solving (4.5)-(4.8) with the larger solution for λ_2^*. The easiest approach therefore is the SFE explained in section 3.1.1. Since our system of equations is quite complex we use the numerically less expensive way of finding the fixed-point value[3] of $\bar{\varepsilon}^*$. Recall that this way was to maximize the ratio c_n/c_{n+1} for large n. The result is shown in figure 4.1. We find five different maxima at the order $n = 14$ but only two of them, namely $\bar{\varepsilon}^* = \{-0.0065, 0.0754\}$, remain at all orders n, meaning that only those correspond to the true fixed points. It is important to check that a maximum is preserved in each order to ensure that it is not a numerical artifact. Both true fixed points exhibit very thin maxima in figure 4.1. They get thinner with rising order. Thus, it is advantageous to choose the order n quite low. In figure 4.1 we see as well that we find one symmetry-breaking ($\bar{\varepsilon}^* < 0$) and one (locally) symmetric potential ($\bar{\varepsilon}^* > 0$). At this point it should be emphasized

[3] We name the mass coefficient c_1 from now on $\bar{\varepsilon}$ as we did in the flow equations.

once again that it is an approximation to use the symmetric flow equations for the symmetry-breaking fixed-point potential. But it is a good one since the differences are small as we show at the end of section 4.2.3. The computation from above can be performed for an arbitrary (N_c, N_f)

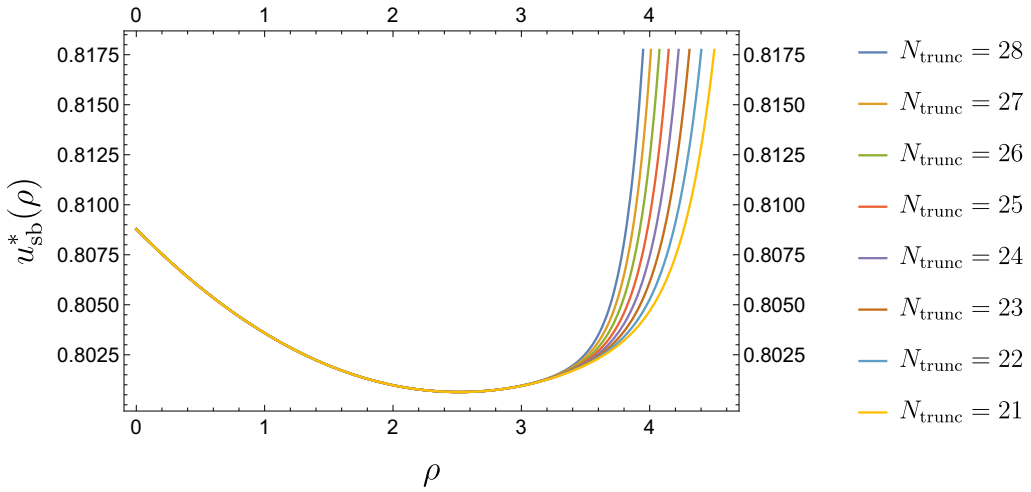

(a) Symmetry-breaking (sb) fixed-point potential, $\bar{\epsilon}^* = -0.0065$.

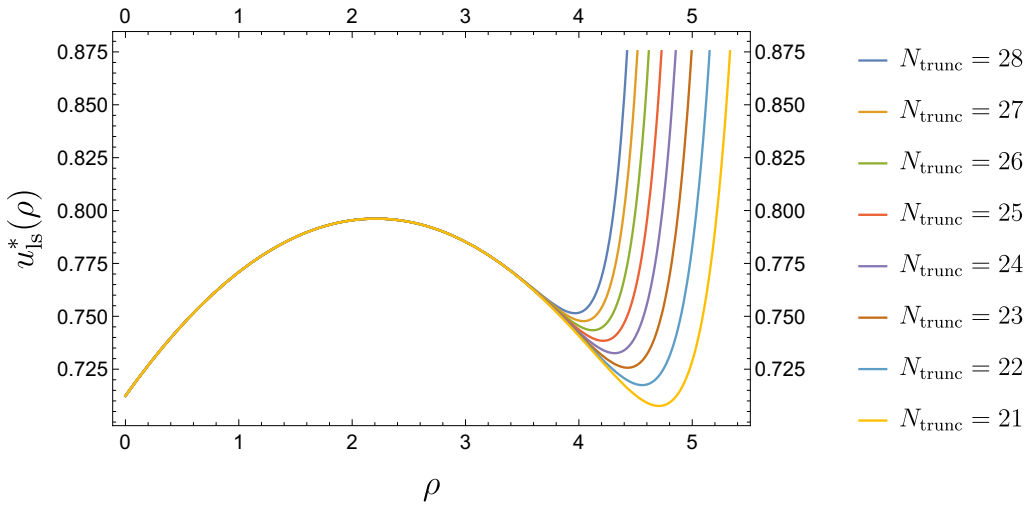

(b) Locally symmetric (ls) fixed-point potential, $\bar{\epsilon}^* = 0.0754$.

Figure 4.2.: Fixed-point potentials computed via small-field expansions for different orders of truncation.

combination (as long as $\epsilon \ll 1$) and we always find two fixed-point values for $\bar{\epsilon}$ with one bigger and one smaller than zero. Explicit values are given in section 4.3. Inserting $\bar{\epsilon}^*$ into the power series ansatz (3.4), we obtain the values for all other couplings like it is described in section 3.1.1. The corresponding fixed-point potentials are shown in figure 4.2. They are plotted for different orders N_{trunc} of the power series ranging from 21 to 28. With increasing order the series diverges closer to the origin. Thus, the radius of convergence of the power series cannot be determined

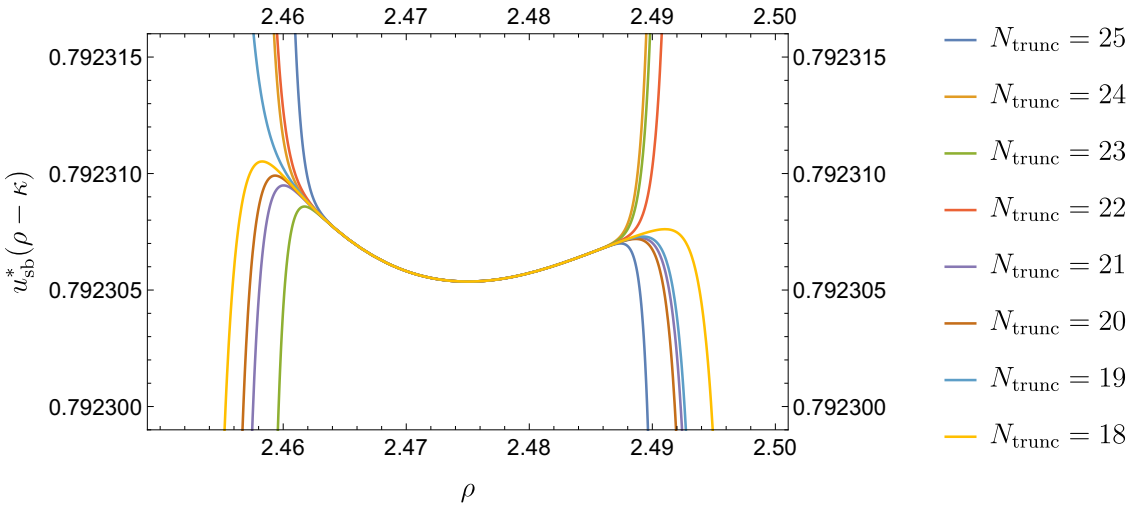

Figure 4.3.: Expanding the fixed-point potential in power of $(\rho-\kappa)$ for different orders of the power series ranging from $N_{\mathrm{trunc}} = 18$ to 25.

using the small-field expansion. The first few orders of the power series read

$$u^*_{\mathrm{sb,SFE}}(\rho) = 0.80878 - 0.0065\rho + \frac{1}{2}\times 0.00262144\rho^2 + \cdots, \tag{4.9}$$

$$u^*_{\mathrm{ls,SFE}}(\rho) = 0.712374 + 0.0754\rho - \frac{1}{2}\times 0.0335146\rho^2 + \cdots, \tag{4.10}$$

where we find the fixed-point couplings for the symmetry-breaking potential to be $\lambda^*_{1,\mathrm{sb}} = 0.00262$, $\lambda^*_{2,\mathrm{sb}} = 0.6024$, $\kappa^* = 2.475$ and for the locally symmetric potential $\lambda^*_{1,\mathrm{ls}} = -0.03351$ and $\lambda^*_{2,\mathrm{ls}} = 0.6655$. We compare those values with the other methods and the perturbative results in table 4.2 and 4.3 of section 4.3. For symmetry-breaking potentials, there is a different ansatz (3.7), often achieving better convergence. The key problem here is the more complex equations to solve due to the incorporation of the non-trivial minimum κ in the anomalous dimensions and the β functions of the couplings. To simplify this higher complexity, we set the anomalous dimensions η_ϕ and η_χ to zero (since $\eta_\phi \ll d$ as shown in section 4.2.3). The location of the fixed-point minimum κ^* is again found by scanning through values of κ and maximizing the ratio c_n/c_{n+1}. We find the potential to be

$$u^*_{\mathrm{sb}}(\rho) = 0.792305 + 0.0163812\times(\rho - 2.475)^2 + \cdots. \tag{4.11}$$

Plotting the potential for different orders of the power series up to $N_{\mathrm{trunc}} = 25$ yields figure 4.3. The location of the minimum $\kappa^* = 2.475$ is in accordance with the other small-field expansion but we only find a solution valid in a small area around the minimum. The radius of convergence is, like before, hard to estimate.
For a better estimation we consult the shooting method as explained in section 3.1.3. The results are depicted in figure 4.4 and they confirm the results of the SFE that two fixed points exist. Furthermore, the shooting suggests radii of convergence for the fixed-point potentials to be $\rho_{\mathrm{s,sb}} = 2.654$ and $\rho_{\mathrm{s,ls}} = 3.821$. Note that there exists a global maximum at $\bar{\epsilon} = -1$ (which is found as well using SFE. This is indicated by the fact that the curve increases for negative ϵ). This leads to a constant, infinite potential which does not satisfy the fixed-point equation (4.8).

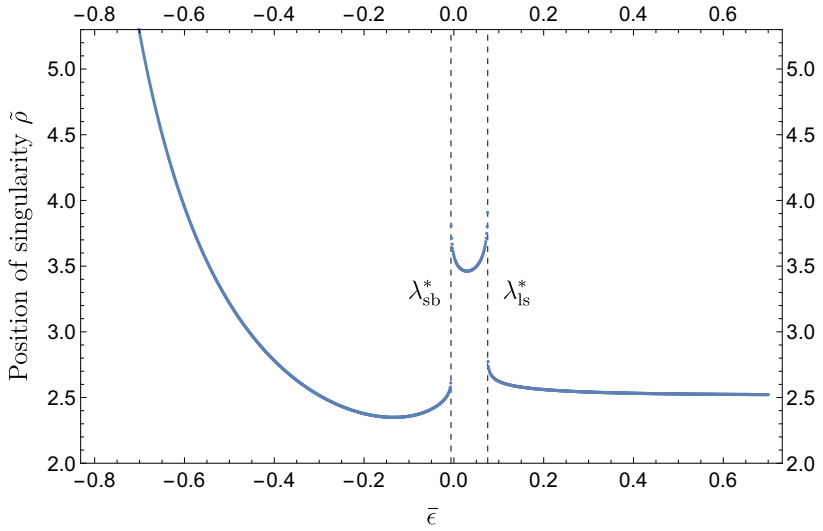

Figure 4.4.: Shooting from the origin up to the location of the movable singularity. Two local maxima exist: $\bar{\varepsilon}^*_{sb} = -0.0065$ and $\bar{\varepsilon}^*_{ls} = 0.0754$.

Armed with the fixed-point values from the small-field expansion and the shooting, the next step is the computation of the fixed-point potential for large field amplitudes for which we use the large-field expansion explained in section 3.1.2. Therefore, we insert the ansatz (3.10)

$$u^*_L(\rho) = A\rho^{N_\infty} + \sum_{i=1}^{2} c_{L,i}\rho^{i(1-N_\infty)} + \sum_{i=0}^{2} \gamma_{L,i}\rho^{-i}, \tag{4.12}$$

into (4.8). We have chosen the truncation order of the power series to be $N_{\text{trunc}} = \widetilde{N}_{\text{trunc}} = 2$ which simplifies the calculation and is enough for our purposes as we will see shortly. We obtain the coefficients $c_{L,i}$ and $\gamma_{L,i}$ in terms of A. The symmetry-breaking potential has the explicit form:

$$u_{\text{LF,sb}} = A\rho^{1.9472} + \frac{0.212546}{A\rho^{0.947204}} + \frac{9.95624}{\rho} - \frac{0.0822396}{A^2\rho^{1.89441}} - \frac{445.793}{\rho^2} + \cdots. \tag{4.13}$$

Setting $A = 1$ for a first impression, we can plot the series (4.13) for different N_{trunc} logarithmically as in figure 4.5. Increasing the order of the power series which we insert into the fixed-point equation, we see a faster diverging solution (seen from the point of expansion which is infinity). Hence, this simple approach already shows that the radius of convergence ρ_A is smaller (again seen from infinity) than 10: $\rho_A > 10$. Thus, there is no possibility to glue together the SFE and LFE since the condition (3.11) cannot be fulfilled ($\rho_s = 2.654 < 10 < \rho_A$). The radii of convergence do not overlap. There is no possibility to construct a global fixed-point potential from the small- and large-field expansions. This is the case independently of the combination (N_c, N_f). Analogously, similar results are obtained for the symmetric fixed-point potential. We do not explicitly show them here because no new insights are gained. To get a global solution, we need a method with better convergence properties which we already have introduced in section 3.1.4: the pseudo-spectral method. Nevertheless, the effort we made up to here was not in vain since we will need the solutions from the small- and large-field expansions to construct an initial guess that is required for the pseudo-spectral method as we will see shortly. In the next section we use and explain its implementation and results in detail.

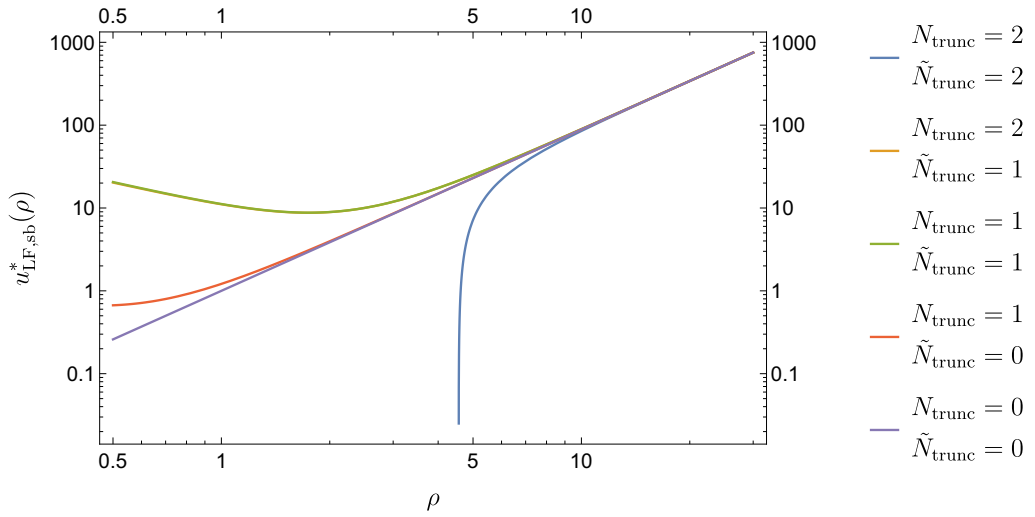

Figure 4.5.: Symmetry-breaking fixed-point potential computed with a LFE plotted logarithmically up to different orders of the power series ansatz for $A = 1$. With increasing order of the power series the solution diverges for higher field amplitudes.

4.2.2. Global fixed-point potentials with pseudo-spectral methods

Due to better convergence properties of Chebyshev polynomials, there is hope that the fixed-point equation (4.8) for the potential can be solved globally using the PSM. Before showing the results, we recap the important steps in the implementation of the method so that it can be reproduced more easily. Whenever we apply the PSM, we will solve the fixed-point equation for u' which is the derivative with respect to ρ of the potential u. The equation for the Gauge-Yukawa theories then reads

$$\begin{aligned} 0 = &- d\,u' + (d-2+\eta_\phi)(\rho u'' + u') - \frac{4v_d}{d}\left(1-\frac{\eta_\phi}{d+2}\right)\left[\frac{(N_\mathrm{f}{}^2-1)(u''+\lambda_2/N_\mathrm{f})}{(1+u'+\frac{\rho\lambda_2}{N_\mathrm{f}})^2} + \frac{N_\mathrm{f}{}^2 u''}{(1+u')^2} + \right. \\ &\left. + \frac{3u''+2\rho u'''}{(1+u'+2\rho u'')^2}\right] + \frac{4v_d}{d} d_\gamma N_\mathrm{c}\left(1-\frac{\eta_\psi}{d+1}\right)\frac{h_\phi^2}{(1+\frac{\rho}{N_\mathrm{f}}h_\phi^2)^2}. \end{aligned} \tag{4.14}$$

At the beginning of the implementation, an initial guess needs to be produced. This guess serves as an initial point in the landscape of possible solutions of the system of algebraic equation that is obtained by the collocation method. The guess has to be "good enough" such that the Newton-Raphson method starts close to the solution we aim at. Numerically, it is a tough exercise to find a solution of a system with many equations due to numerical artifacts. Therefore the staring point needs to be a good one. In our case the small- and large-field expansions are the ideal candidates for this because we know that they are (on their validity interval) the solutions we search for. To construct those initial guesses we connect the SFE (valid up to ρ_s) and the LFE (valid from ρ_L to infinity) with a parabola in such a way that at the connection points ρ_s and ρ_L the functions are connected smoothly. This is needed as we strive for a global fixed-point potential. Therefore, a globally defined initial guess is necessary. The next step is to divide the guess into the M parts. Each part is then transformed into the interval $[-1,1]$ with a suitable affine transformation[4] which is given in section 3.1.4. Furthermore, diverging parts (which is in

[4] Keep in mind that the derivatives transform as well.

our case the last part as it ranges up to infinity) need to be rescaled by their asymptotic behavior before transforming them to $[-1,1]$. Rescaling means to divide the fixed-point equation and the initial guess by a factor of $(1+\rho^{N_\infty-1})$ with N_∞ the asymptotic behavior of the solution u. The exponent $N_\infty - 1$ appears because we solve the fixed-point equation for u' which changes the asymptotic behavior respectively. Note that multiple possibilities arise here. For example, we could rescale the whole initial guess or just the diverging parts. Later on, we will find that in our computations the latter possibility will give the best solution. The following step is to expand the initial guesses on the M parts into Chebyshev polynomials of order n. We do the same for an array of coefficients. Those coefficients will serve as the variables of our system of equation on which we will apply the Newton-Raphson method. We use an array of coefficients for each of the M parts and compute their derivatives with the derivative algorithm (3.17). Inserting the array and its derivatives of each part into the corresponding fixed-point equation and applying the collocation method for a suitable number of collocation points[5], results in a system of algebraic equations. Together with the $p \times (M-1)$ matching conditions (where p is the order of the ODE) we obtain a system of $M \times n$ algebraic equations for the $M \times n$ coefficients which we solve using Newton-Raphson. After the inverse affine transformation and suitable rescaling we end up with a solution of the fixed-point equation.

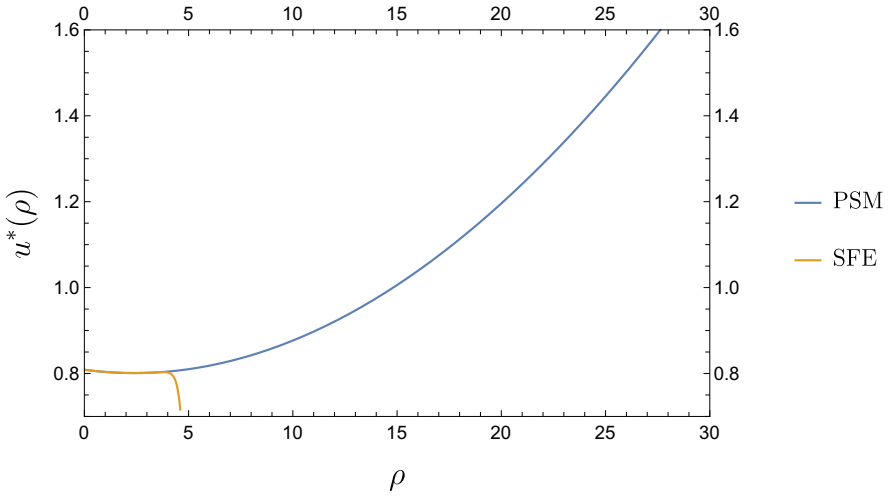

Figure 4.6.: Symmetry-breaking fixed-point potential in SFE (yellow) to order $N_{\text{trunc}} = 15$ and in PSM (blue) to order 40. The PSM exhibits a global solution which is bounded from below.

At first, we apply this prescription onto the symmetry-breaking fixed point. There, we divide the ansatz into $M = 2$ parts with the matching point $\rho_s = 2.7$ which is also the point up to which the SFE is valid such that the matching point includes the non-trivial minimum at $\rho = 2.475$. Furthermore, we build the initial guess from $\rho_L = 10$ on with the LFE and use for the compactification parameter $L = 20$. For the initial guess we use the corresponding derivative of the SFE of order $N_{\text{trunc}} = 15$ and LFE of order $N_{\text{trunc}} = 1$. It is advantageous to choose N_{trunc} not too large for the initial guess because then the series does not diverge too fast. With these parameters we can carry out the calculation.

[5]The suitable number in this context means that we need $Mn - p(M-1)$ collocation points on M parts in total.

The results are shown in figure 4.6, the blue curve represents the PSM to order 40 and the yellow curve the SFE to order 15. The first few orders of the fixed-point potential computed with the PSM read

$$u^*_{\text{sb,PSM}}(\rho) = 0.80878 - 0.0065071\rho + \frac{1}{2} \times 0.0027624\rho^2 + \cdots . \tag{4.15}$$

The solution with the PSM does not diverge as it is the case for the SFE. We obtain a global solution which is indeed smooth at the matching point $\rho_s = 2.7$ and bounded from below. The Gauge-Yukawa theories exhibit a global, symmetry-breaking fixed-point potential in the scalar section which is bounded from below. This confirms and extends the perturbative stability analysis of [1] which is valid up to power H^4. Thus, an important consistency check for high-energy complete QFTs is fulfilled.

We can perform the same calculations for the fixed point in the symmetric regime where $\bar{\varepsilon} = 0.0754$. We choose the parameters to be $\rho_s = 4$ which is again as well the matching point, $\rho_L = 20$ and $L = 20$. The SFE and LFE are as before smoothly connected with a parabola. The resulting

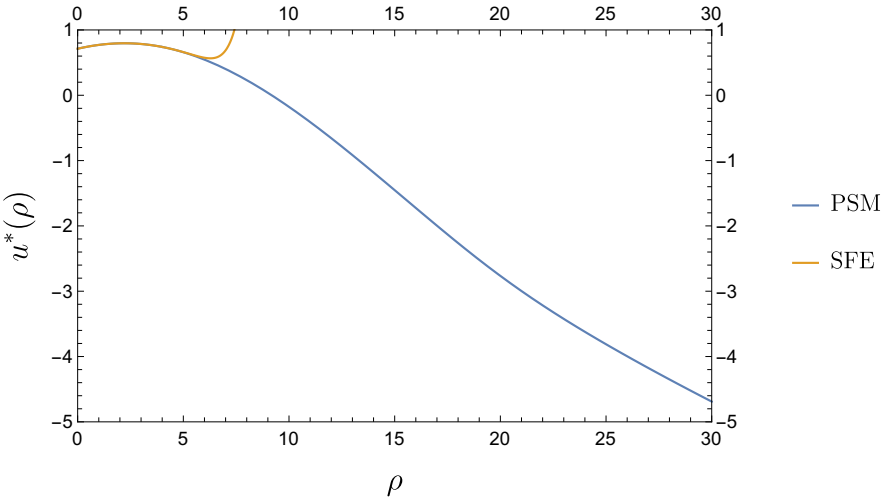

Figure 4.7.: Locally symmetric fixed-point potential in SFE (yellow) to order $N_{\text{trunc}} = 15$ and in PSM (blue) to order 30. The PSM exhibits a global but unbounded solution.

fixed-point potential is given in figure 4.7 up to 30 expansions coefficients. It is again a global result and its numerical expansion starts with

$$u^*_{\text{ls,PSM}}(\rho) = 0.712374 + 0.0754065\rho - \frac{1}{2} \times 0.033495\rho^2 + \cdots . \tag{4.16}$$

This potential has the unphysical property to be unbounded from below but it is globally defined. This potential might only serve as a local and effective model. Nevertheless, apart all mathematical issues, this potential is from a phenomenological perspective uninteresting since all fermions would be massless and thus are degrees of freedom of the theory.

4.2.3. Error analysis

In the previous section, we found two global fixed-point potentials. This section is dedicated to the error analysis of these potentials. A good indication for how accurate a solutions is, is obtained from plugging it into the fixed-point equation for u'. For the symmetry-breaking potential (4.15) we find figure 4.8 (a) for the interval $[0, \rho_s]$ where the residual oscillates between

-4×10^{-12} and 4×10^{-12} for a potential of order $N_{\text{trunc}} = 40$. For a potential of order 30 we find residuals of about 10^{-10}. This shows that the residual on these truncation orders and thus the error of the potential still continues to decrease. In contrast to the solution for large fields on

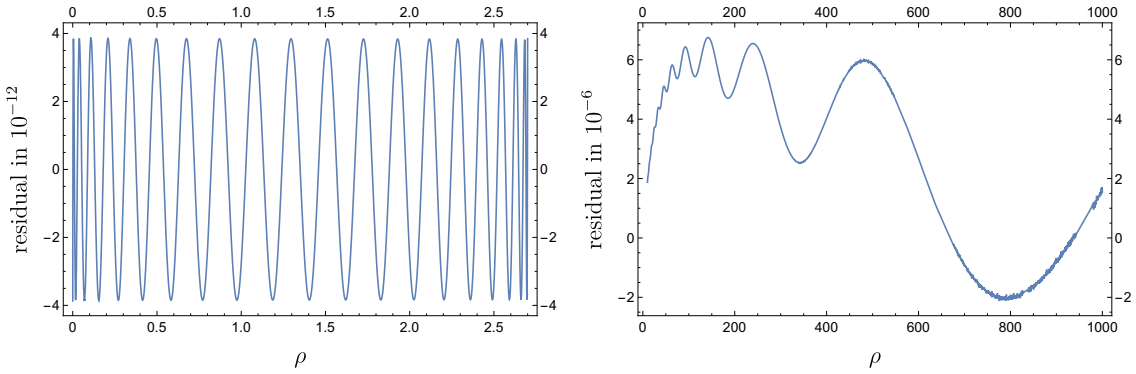

(a) Chebyshev expansion in $\rho \in [0, \rho_s]$.

(b) Rational Chebyshev expansion in $\rho \in [\rho_s, \infty]$.

Figure 4.8.: Inserting the solutions from PSM into the fixed-point equation for u' for $\rho \in [0, \infty]$.

$\rho \in [\rho_s, \infty]$ where the residual is plotted in figure 4.8 (b). The residuals are of order 10^{-6} with a maximal value of 6×10^{-6}. For the order 30 we find the residuals to be of the same order and just slightly larger since the maximal value is 8×10^{-6}. Thus, the PSM for small fields yields better results than the one for large fields. One reason might be the rescaling in the large field case with the corresponding fractional exponents (since $\eta_\phi \neq 0$). Following this line of argument, potentials up to higher orders might be worth computing for small field values and not for large field values if higher accuracy is needed. Similar calculations for the solution via the SFE show by far not as accurate results as the PSM.
The same analyses were carried out for the locally symmetric potential, where we find that the residuals are larger for small and large field values. At order 40 we find residuals of order 10^{-7} for small field values and 10^{-5} for large field values. A reason for the discrepancy compared to the symmetry-breaking regime especially for small field values is unknown but could be numerical. Another interesting analysis is to plot the coefficients over their order logarithmically where the kind of convergence of the coefficients can be detected. This is done up to order 40 for the symmetry-breaking case and the results are shown in figure 4.9. There, $u'(\rho)$ with $\rho \in [0, \rho_s]$ is expanded in a Chebyshev series of order 40 and $u'(\rho)/\rho^{(2-\eta_\phi)/(2+\eta_\phi)}$ in a rational Chebyshev series of the same order. We see exponential convergence for the ordinary Chebyshev expansion (the curve bends down) whereas for the rational expansion approximately at order $n = 20$ algebraic convergence kicks in. The reason for this is that due to the non-vanishing anomalous dimensions the potential rises with fractional power. Furthermore, the fact that the absolute value of the coefficients is smaller for the ordinary Chebyshev expansion reflects the fact that its error is smaller as we saw above.
We also computed the fixed-point potentials by dividing the solution into more than $M = 2$ parts. This leads to a slightly better convergence (approximately one order of magnitude in the coefficients) in the transition area where SFE and LFE are not valid.

Finally, we want to justify the approximation we have done in several computations regarding the anomalous dimensions: Either to set them to zero or to use their symmetric flow equations (instead of the symmetry-breaking equations) in the symmetry-breaking regime. If we look at the absolute numbers of the anomalous dimensions in both regimes we find the values $\eta_\phi(\rho =$

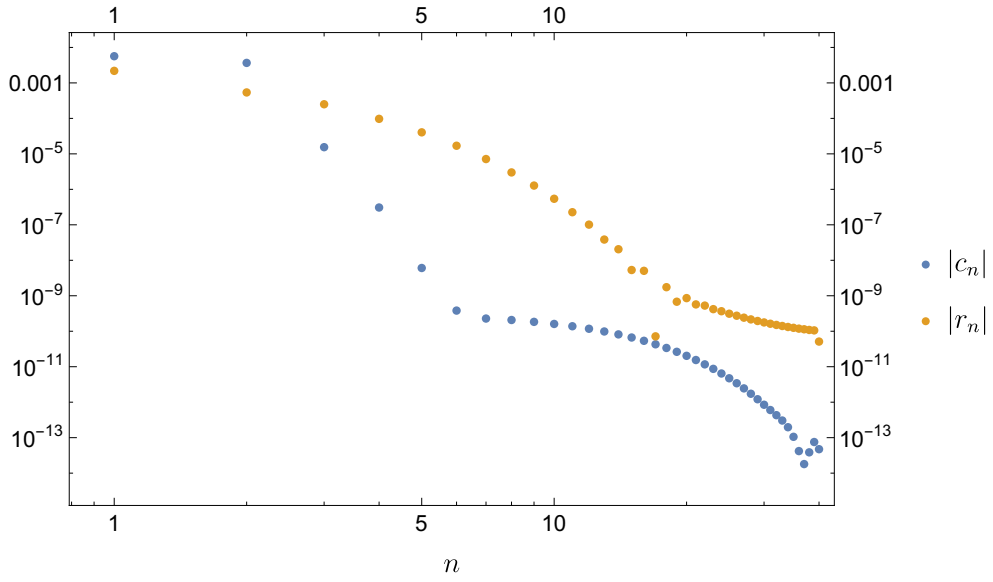

Figure 4.9.: Decay of the coefficients of Chebyshev series (blue) in $[0,\rho_s]$ and of rational Chebyshev series (yellow) in $[\rho_s,\infty]$ of the derivative of the symmetry-breaking fixed-point potential.

0) = 0.04553, $\eta_\chi(\rho=0)=0.13798$ at the origin and $\eta_\phi(\rho=\kappa^*)=0.04532$, $\eta_\chi(\rho=\kappa^*)=0.15872$ at the non-trivial minimum κ^* using the equations (2.66) and (2.67). We find that they are small compared to the spacetime dimension and that the differences of both regimes are small too. To minimize the error of this approximation one could invent an iterative procedure: Calculate the non-trivial minimum of the fixed-point potential and insert the values of the anomalous dimensions at this minimum into a new computation to obtain a more accurate potential with a sightly different located minimum and perform the same calculation as long as the location of the minimum changes up to a chosen accuracy.

4.3. Other (N_c, N_f) configurations

In the last section we specified our calculations to the special configuration $(N_c,N_f)=(5,28)$ which we want to generalize in this section to other configurations. Since everything from section 4.2.2 applies to other (N_c,N_f) as well, the results will only be briefly summarized in the following. An exemplary symmetry-breaking fixed-point potential with a smaller $\epsilon = 1/106$ (or $(N_c,N_f)=(53,292)$) is shown in figure 4.10. We observe that the non-trivial minimum has changed its location to the field value $\kappa^* = 228.87$ which is significantly bigger than the one for the configuration (5,28) ($\epsilon = 1/10$). This makes the calculation of the potential numerically more difficult, as the interval up to the matching point is larger. Moreover, the coupling κ seems to increase with decreasing ϵ. This effect is examined in detail in section 4.4. The numerical expansion of the fixed-point potential in SFE and PSM shown in figure 4.10 is given by

$$u^*_{\mathrm{sb,SFE}}(\rho) = 86.0693 - 0.000497\rho + \frac{1}{2}\times 2.1959\times 10^{-6}\rho^2 + \cdots, \tag{4.17}$$

$$u^*_{\mathrm{sb,PSM}}(\rho) = 86.0693 - 0.00049643\rho + \frac{1}{2}\times 2.199998\times 10^{-6}\rho^2 + \cdots. \tag{4.18}$$

We can compare the values of the couplings for different (N_c,N_f) and different methods with the perturbative results of [1]. The results for the symmetry-breaking fixed point are summarized

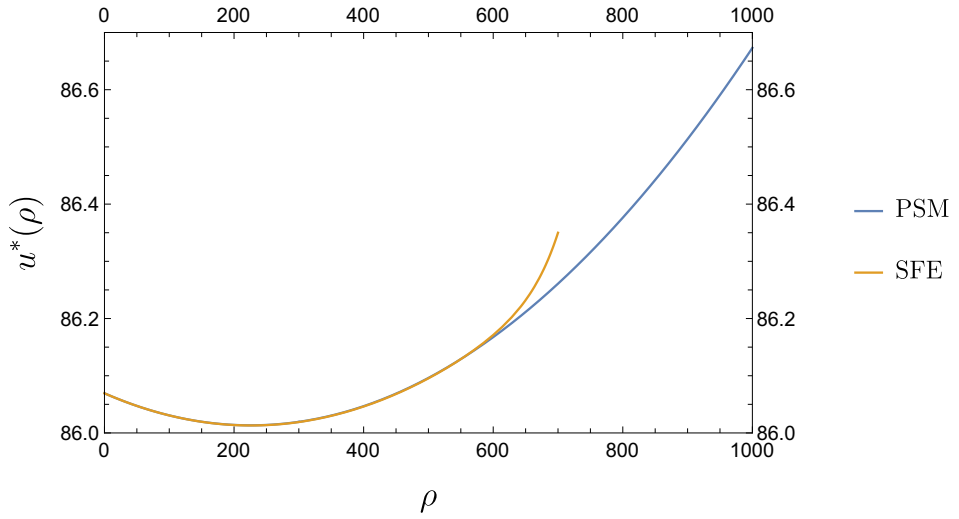

Figure 4.10.: Symmetry-breaking fixed-point potential for the configuration $(N_c, N_f) = (53, 292)$ in SFE (yellow) to order $N_{\text{trunc}} = 20$ and in PSM (blue) to order 30. The PSM exhibits a global solution.

in table 4.2. For the couplings $\lambda^*_{2,\text{SFE}}$ and $\lambda^*_{2,\text{PSM}}$ we have taken the same value since their differences are minimal. The couplings decrease with decreasing ϵ as the perturbative calculation suggests. In addition, the differences in the results compared to the perturbative results also

Table 4.2.: Overview of the values of the couplings computed with different methods of the symmetry-breaking fixed-point potential for different values of ϵ. The abbreviation 'LS' indicates the perturbative results obtained by [1].

ϵ	$\bar{\varepsilon}^*_{\text{SFE}}$	$\bar{\varepsilon}^*_{\text{PSM}}$	$\lambda^*_{1,\text{SFE}}$	$\lambda^*_{1,\text{PSM}}$	$\lambda^*_{1,\text{LS}}$	$\lambda^*_{2,\text{SFE/PSM}}$	$\lambda^*_{2,\text{LS}}$	κ^*
$\frac{1}{10}$	-0.0065	-0.00651	0.00262	0.00276	0.00537	0.60239	0.61061	2.45
$\frac{1}{22}$	-0.002582	-0.00241	0.000247	0.000237	0.000346	0.10621	0.10682	10.67
$\frac{1}{106}$	-0.000497	-0.000496	2.196×10^{-6}	2.2×10^{-6}	2.357×10^{-6}	0.00415	0.00418	228.87
$\frac{1}{500}$	-0.00010375	-	5.2164×10^{-9}	-	5.3013×10^{-9}	9.219×10^{-5}	9.222×10^{-5}	19959.8
$\frac{1}{10000}$	-5.1785×10^{-6}	-	6.5276×10^{-13}	-	6.5304×10^{-13}	2.2947×10^{-7}	2.2952×10^{-7}	7.941×10^{6}

decrease. This shows that the perturbative results are increasingly justified with decreasing ϵ (with exception of the non-trivial minimum κ^*). We have not calculated the potentials with the PSM for very small ϵ since the differences to both other methods are nearly vanishing and with decreasing ϵ it gets increasingly difficult to use the PSM due to large numbers in the numerics. For a detailed study, a rescaling of the field amplitude with a suitable power of ϵ might be useful. Moreover, we have good confidence from all other examples that the fixed-point potential exists globally. For the locally symmetric fixed-point potential we summarize the results in table 4.3 where we make the same observations independently of (N_c, N_f). The couplings decrease with diminishing ϵ and the nonperturbative results approach the perturbative ones.

Table 4.3.: Overview for the locally symmetric fixed-point potential for different values of ϵ.

ϵ	$\bar{\varepsilon}^*_{\mathrm{SFE}}$	$\bar{\varepsilon}^*_{\mathrm{PSM}}$	$\lambda^*_{1,\mathrm{SFE}}$	$\lambda^*_{1,\mathrm{PSM}}$	$\lambda^*_{1,\mathrm{LS}}$	$\lambda^*_{2,\mathrm{SFE/PSM}}$	$\lambda^*_{2,\mathrm{LS}}$
$\frac{1}{10}$	0.0754	0.07541	-0.0335	-0.0335	-0.0242	0.67225	0.61061
$\frac{1}{22}$	0.03277	0.03258	-0.002885	-0.002863	-0.00249	0.1113	0.10682
$\frac{1}{106}$	0.006516	0.006433	-2.401×10^{-5}	-2.369×10^{-5}	-2.333×10^{-5}	0.00421	0.00418
$\frac{1}{500}$	0.0013695	-	-5.6381×10^{-8}	-	-5.6045×10^{-8}	9.2355×10^{-5}	9.222×10^{-5}
$\frac{1}{10000}$	3.8335×10^{-5}	-	-7.0229×10^{-12}	-	-7.0205×10^{-12}	2.2948×10^{-7}	2.2952×10^{-7}

Finally, let us now focus on the dependency of the mass coupling $\bar{\varepsilon}^*$ of ϵ. We will only study the locally symmetric case since both are similar and results for the non-trivial minimum κ^* at the fixed point are presented in section 4.4. Inserting the threshold integrals of appendix B, we write (2.70) at the fixed point as

$$0 = -(2-\eta_\phi)\bar{\varepsilon} - \frac{4v_d}{d}\left\{\left[2(N_\mathrm{f}^2-1)\lambda_1 + \frac{N_\mathrm{f}^2+1}{N_\mathrm{f}}\lambda_2\right]\left(1-\frac{\eta_\phi}{d+2}\right)\frac{1}{(1+\bar{\varepsilon})^2} - d_\gamma N_\mathrm{c} h_\phi^2\left(1-\frac{\eta_\chi}{d+1}\right)\right\}. \quad (4.19)$$

Inserting the perturbative dependencies

$$\lambda_1^* \propto \frac{\epsilon}{{N_\mathrm{f}}^2}, \quad \lambda_2^* \propto \frac{\epsilon}{N_\mathrm{c}}, \quad h_\phi^{2*} \propto \frac{\epsilon}{N_\mathrm{c}}, \quad N_\mathrm{f} \propto \frac{1}{\epsilon}, \quad N_\mathrm{c} \propto \frac{1}{\epsilon}, \quad (4.20)$$

of the fixed point couplings of ϵ into (4.19) and setting the anomalous dimensions to zero since $d \gg \eta_i$ results in the dependency

$$\bar{\varepsilon} \propto \epsilon + \epsilon^2 + \cdots \quad (4.21)$$

to leading order. We see this graphically as well in figure 4.11. Here, a parabolic fit is applied since the order ϵ^2 is important for bigger ϵ. Nevertheless, for very small ϵ the linear order dominates.

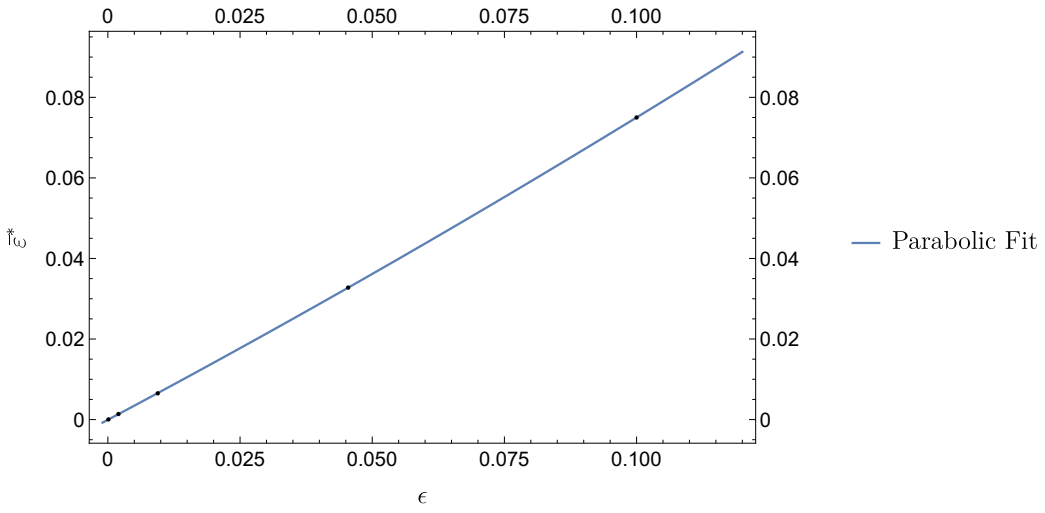

Figure 4.11.: Fixed-point mass coupling $\bar{\varepsilon}^*$ plotted as a function of $\epsilon = N_\mathrm{f}/N_\mathrm{c} - 11/2$. We observe a linear dependency to leading order for small ϵ.

4.4. An interesting nonperturbative effect

In this section the fixed-point structure of the non-trivial minimum κ is investigated. In particular, its dependency on the parameter $\epsilon = N_f/N_c - 11/2$ is studied. For this, a good starting point is the flow equation (2.73) of κ:

$$\begin{aligned}\partial_t \kappa =& (2-d-\eta_\phi)\kappa + 2v_d\Big\{ {N_f}^2 l_1^2(0;\eta_\phi) + 3l_1^d(2\lambda_1\kappa;\eta_\phi) \\ &+ ({N_f}^2-1)\left(1+\frac{\lambda_2}{\lambda_1 N_f}\right) l_1^d\left(\frac{\lambda_2\kappa}{N_f};\eta_\phi\right) - d_\gamma N_c \frac{h_\phi^2}{\lambda_1} l_1^{(F)d}\left(\frac{h_\phi^2\kappa}{N_f};\eta_\chi\right)\Big\}.\end{aligned} \tag{4.22}$$

To investigate possible fixed points κ^*, we set the anomalous dimensions η_ϕ, η_ψ (which are of order $10^{-1} \ll d$ with d the spacetime dimension as computed in section 4.2.3) to zero for simplicity. With these simplifications and the explicit formulas for the threshold functions from

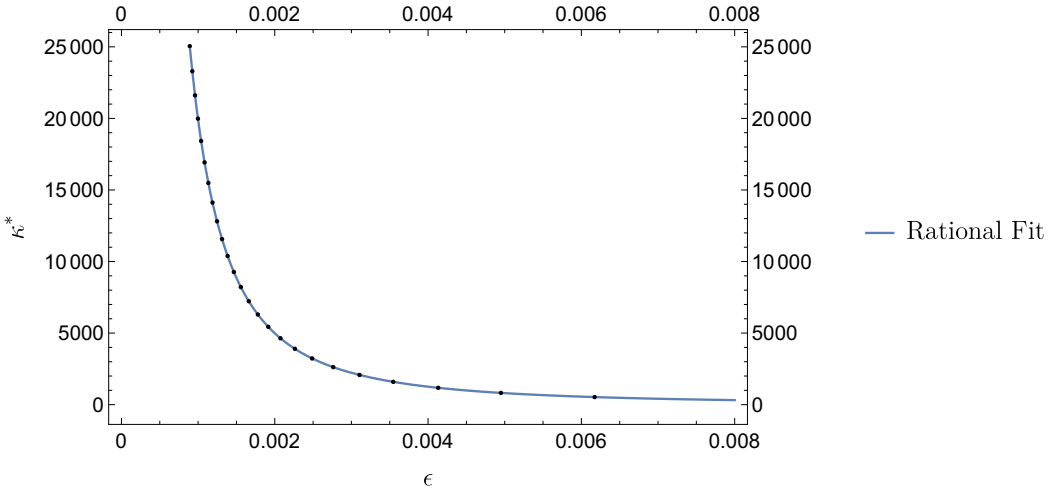

Figure 4.12.: Position of the non-trivial minimum κ^* as a function of $\epsilon = N_f/N_c - 11/2$. With decreasing epsilon the minimum increases quadratically. The curve is fitted with a rational fit.

appendix B the equation at the fixed point reads

$$(2-d)\kappa + v_d\left(-\frac{4h_\phi^2 N_c}{\lambda_1\left(1+\frac{h_\phi^2\kappa}{N_f}\right)^2} + {N_f}^2 + \frac{3}{(1+2\kappa\lambda_1)^2} + \frac{({N_f}^2-1)\left(1+\frac{\lambda_2}{\lambda_1 N_f}\right)}{\left(1+\frac{\kappa\lambda_2}{N_f}\right)^2}\right) = 0\,. \tag{4.23}$$

Since we are interested in how the non-trivial fixed-point minimum κ^* and ϵ are related, we insert the proportionality

$$\lambda_1^* \propto \frac{\epsilon}{{N_f}^2},\quad \lambda_2^* \propto \frac{\epsilon}{N_c},\quad h_\phi^{2*} \propto \frac{\epsilon}{N_c},\quad N_f \propto \frac{1}{\epsilon},\quad N_c \propto \frac{1}{\epsilon}, \tag{4.24}$$

with respect to ϵ into (4.23). They follow from the definition of ϵ, (2.36) and (2.37). The relations of λ_1^* and λ_2^* originate from the perturbative calculations. We obtain the dependence

$$\kappa^* \propto \epsilon^{-2}. \tag{4.25}$$

The responsible and dominant terms for this scaling are the terms proportional to N_f^2 and the term $(2-d)\kappa$ in (4.23). Graphically, we can confirm this by computing explicit values for κ^* when setting N_f and N_c to suitable numbers such that $\epsilon \ll 1$. We find figure 4.12 where the black data points are fitted with a rational fit of the form

$$F(\epsilon) = -0.21 + \frac{0.057}{\epsilon} + \frac{0.02}{\epsilon^2} + \frac{4\times 10^{-11}}{\epsilon^3} + \frac{10^{-14}}{\epsilon^4}. \tag{4.26}$$

The errors are suppressed because we are only interested in the proportionality. The fit underlines the $\kappa^* \propto \epsilon^{-2}$ proportionality since the coefficients of the higher orders are almost zero and are likely to be numerical artifacts. Furthermore, for small ϵ the term $1/\epsilon^2$ dominates. Thus, κ^* increases quadratically with decreasing ϵ. We can interpret this physically. Perturbatively speaking, all couplings are supposed to be small with decreasing ϵ, like it is the case for example for g^{2*} or λ_1^* . For κ^* this is not the case; it increases quadratically. This contradicts the implicit assumption that it suffices to study perturbation theory in the deep Euclidean regime where all mass-scale related parameters are assumed to be very small. We found a fully nonperturbative effect of the Gauge-Yukawa system.

Now that we know the dependence of κ^* on ϵ, we dedicate the end of this section to the dependence of the radial mass mode $2\kappa^*\ u''\big|_{\rho=\kappa^*}$ (which may also be called a Higgs mode mass) and the squared fermion mass $h_\phi^{2*}\kappa^*/N_f$ on ϵ. Both mass modes are important quantities of the flow equation of the scalar potential. We start with the radial mass mode where we expect a linear dependence to leading order in ϵ since we already know (perturbatively) the proportionality $\lambda_1^* \propto \epsilon^3$ and $\kappa^* \propto \epsilon^{-2}$. The value $u''\big|_{\rho=\kappa^*}$ is strongly related to the coupling λ_1^*. Therefore

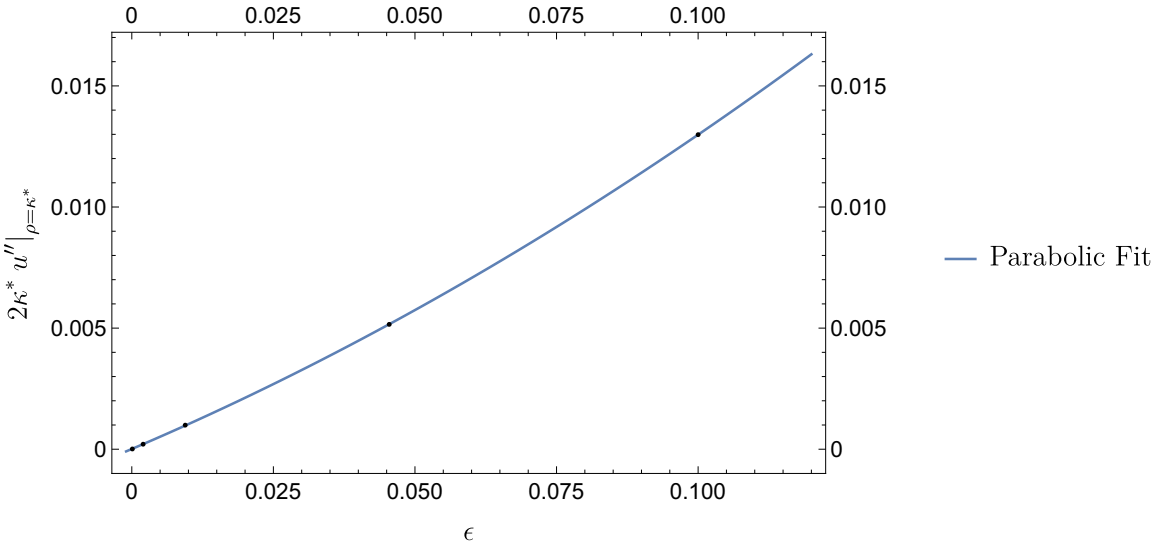

Figure 4.13.: Radial mass mode $2\kappa^*\ u''\big|_{\rho=\kappa^*}$ plotted as a function of $\epsilon = N_f/N_c - 11/2$. We observe a linear dependency to leading order for small ϵ.

$2\kappa^*\ u''\big|_{\rho=\kappa^*} \propto \epsilon + \mathcal{O}(\epsilon^2)$ which is confirmed by figure 4.13 where we have fitted with

$$F(\epsilon) = 10^{-5} + 0.1\epsilon + 0.3\epsilon^2. \tag{4.27}$$

We have suppressed again the errors since we are interested in the proportionality an fitted with a parabola. The offset $F(\epsilon = 0)$ could occur due to the small number of data points used for the

fit. Thus, radial mass modes are controlled by the Veneziano limit like all other couplings except κ^*. Since the Higgs mass parameter can be considered as a measure for the massive deformation of the propagators beyond the Deep Euclidean region, the system nevertheless approaches the perturbative limit despite violating the assumption underlying a mass independent analysis.

Also for the squared fermion mass we expect and find a linear dependence of ϵ to leading order since $h_\phi^{2*} \propto \epsilon^2$, $\kappa^* \propto \epsilon^{-2}$ and $N_\mathrm{f} \propto \epsilon^{-1}$. Thus, also the squared fermion mass is controlled by the Veneziano limit.

4.5. Critical exponents

Critical exponents describe the behavior of physical quantities like the coupling constants in the vicinity of phase transitions or fixed points. They are universal macroscopic properties and thus important characteristics of the system. For these reasons they are the topic of this section. In section 2.2 we already mentioned how to calculate the critical exponents. They are the negative eigenvalues of the stability matrix (2.10) at the fixed point.

We summarize the critical exponents of the system $(\bar{\varepsilon}^*, \lambda_1^*, \lambda_2^*, h_\phi^{2*}, g^{2*})$ of couplings for different ϵ in the table 4.4 where they are as well compared with the perturbative results of [1]. We have used the nonperturbative fixed-point values for λ_1^*, λ_2^* and $\bar{\varepsilon}^*$ of the sections above and the perturbative results for h_ϕ^{2*} and g^{2*}. Relevant eigendirections are negative as explained in section 2.2. For the symmetry-breaking fixed point, we find, in addition to the relevant eigendirection associated with the gauge coupling that is found perturbatively, a relevant direction connected to the mass coupling. All exponents are less than one except for the critical exponent corresponding to the mass coupling and decrease with decreasing ϵ as we expect it from perturbative calculations. The nonperturbative numbers differ from the perturbative ones since we were using nonperturbative fixed-point values in the scalar sector. They differ in the Gauge-Yukawa sector because the single-trace coupling λ_2 influences this sector through the β function of h_ϕ^2 (see (2.28)). Another reason for the differences may come from the fact that we include additional $1/N_\mathrm{f}$ terms. The computations with fixed-point values from SFE and PSM are similar due to their small differences. For the nonperturbative methods we also included the mass coupling $\bar{\varepsilon}$ which does of course not exist for perturbative computations. The corresponding critical exponent is negative and slightly bigger than two which makes it a relevant direction. In the standard model we find a critical exponent of two for the Higgs mass which is directly related to one of the fine-tuning problems. Since for a small number of fermions the fine-tuning problem might be attenuated (absolute value of the critical exponent is less than 2) we will have a closer look at this critical exponent. The other exponents converge towards the perturbative results (2.38)-(2.41) with decreasing ϵ as the values of the couplings did. For the critical exponents in the locally symmetric regime we find the last column in table 4.3. The differences compared to the symmetry-breaking results are the following. We find two relevant directions as in the perturbative regime in addition to the relevant direction corresponding to the mass coupling. This exponent is slightly smaller than two but increases with decreasing ϵ. This enhances the fine-tuning problem for small fermion numbers.
To make the evolution of the critical exponent a little more quantitative we can again look at the dependency of the exponent of ϵ. In both cases, we find to leading order a linear dependency as one would have expected from (4.21) where the subleading order ϵ^2 again influences bigger values of ϵ.

Table 4.4.: Critical exponents for both fixed points of the system of couplings $(\bar{\epsilon}^*, \lambda_1^*, \lambda_2^*, h_\phi^{2*}, g^{2*})$ computed with different methods for different values of ϵ.

ϵ	Symmetry-breaking fixed point	Locally symmetric fixed point
	Small-field expansion	Small-field expansion
$\frac{1}{10}$	$(-1.8418, 0.6552, 0.3969, 0.327, -0.00349)$	$(-2.1567, 0.5856, -0.2002, 0.332, -0.006715)$
$\frac{1}{22}$	$(-1.9317, 0.2284, 0.149, 0.1344, -0.0012088)$	$(-2.0715, 0.2145, -0.1185, 0.1364, -0.001285)$
$\frac{1}{106}$	$(-1.9861, 0.03971, 0.02812, 0.02629, -0.000054034)$	$(-2.0141, 0.03922, -0.02715, 0.02633, -0.00005415)$
$\frac{1}{500}$	$(-1.9973, 0.00815, 0.0054, 0.00532, -2.431 \times 10^{-6})$	$(-2.003, 0.00813, -0.00585, 0.0055, -2.431 \times 10^{-6})$
$\frac{1}{10000}$	$(-1.9999, 0.000404, 0.000294, 0.000274, -6.078 \times 10^{-9})$	$(-2.0002, 0.000404, -0.000294, 0.000274, -6.078 \times 10^{-9})$
	Pseudo-spectral method	Pseudo-spectral method
$\frac{1}{10}$	$(-1.8418, 0.6552, 0.3969, 0.327, -0.00349)$	$(-2.1567, 0.5856, -0.2002, 0.332, -0.006715)$
$\frac{1}{22}$	$(-1.9317, 0.2284, 0.149, 0.1344, -0.0012088)$	$(-2.071, 0.2145, -0.1169, 0.1364, -0.001285)$
$\frac{1}{106}$	$(-1.9861, 0.03971, 0.02812, 0.02629, -0.000054034)$	$(-2.0138, 0.03923, -0.00265, 0.02634, -0.00005415)$
	Perturbative results	Perturbative results
$\frac{1}{10}$	$(0.6146, 0.4362, 0.3585, -0.002539)$	$(0.6146, -0.1518, 0.3585, -0.002539)$
$\frac{1}{22}$	$(0.212, 0.1584, 0.1401, -0.001135)$	$(0.212, -0.1089, 0.1401, -0.001135)$
$\frac{1}{106}$	$(0.03947, 0.02867, 0.02643, -0.00005346)$	$(0.03947, -0.0268, 0.02643, -0.00005346)$
$\frac{1}{500}$	$(0.00814, 0.00592, 0.0055, -2.425 \times 10^{-6})$	$(0.00814, -0.00584, 0.0055, -2.425 \times 10^{-6})$
$\frac{1}{10000}$	$(0.000404, 0.000294, 0.000274, -6.077 \times 10^{-9})$	$(0.000404, -0.000294, 0.000274, -6.077 \times 10^{-9})$

4.6. Fixed-point potentials in τ direction

So far, we have focused our calculations on potentials and fixed points in the direction of the invariant ρ, keeping only the influence of the linear τ term, namely the coupling λ_2. We specialized our calculations in this fashion to obtain an ODE and since the ρ direction is important for giving the fermions their masses. Nevertheless, similar computations can be performed in the direction of τ, taking into account a term proportional to τ^2 which changes the mass spectrum of scalar fluctuations. To obtain an ODE again, we keep the couplings λ_1 and $\bar{\varepsilon}$ in the symmetric case as small influences. This time we need to keep the coupling of ρ^2 as well since it is important for the radial masses.
The mass spectrum is computed in appendix A.2. It is the same as table 2.1 except for the last to eigenvalues. These are the only ones depending on second derivatives of the potential and are therefore the only ones that change. In this work the fixed-point potentials were not constructed for the following reasons. The scalar potential of the Gauge-Yukawa theories with N_f fermions depend in general on N_f invariants as we have mentioned in section 2.3. The τ direction (which is in the nomenclature of (2.20) τ_2) is thus only one of many equivalent directions to study. The gained insights are therefore expected to be small.

5. Summary and Outlook

In this work, Gauge-Yukawa theories discussed by Litim and Sannino in [1] and earlier papers are investigated nonperturbatively regarding their fixed points and scalar potentials. The Gauge-Yukawa theories show an interacting UV fixed point which makes the theories asymptotically safe. Moreover, they have the special property of being accessible perturbatively in the Veneziano limit. Due to the asymptotically safe nature of the Gauge-Yukawa theories, they are good candidates for high-energy complete and consistent QFTs. Thus, they could solve problems of the Standard Model and could serve as theories beyond it. An important criterion for consistent QFTs is the global stability and existence of the scalar potential which has not been explored for the Gauge-Yukawa theories so far which makes it the pivotal point of our investigations.

Since a global stability analysis requires nonperturbative methods, we use the framework of Functional Renormalization Group for all of our computations, in particular the Wetterich equation [15] which follows from basic FRG. The Wetterich's equation is used to derive flow equations which form the basis of all investigations regarding the fixed points at the associated potentials. The fixed-point potentials are computed with small- and large-field expansions, numerical shooting and pseudo-spectral methods for several numbers N_f of fermions and gauge fields N_c.

Nonperturbatively, we find the same two fixed points that were found perturbatively by [1] independently of the combination of $(N_\mathrm{c}, N_\mathrm{f})$ (as long as $\epsilon \ll 1$). One fixed point is symmetry breaking whereas the other one is locally symmetric. With decreasing ϵ the difference between the nonperturbative and perturbative results diminishes as expected. The symmetry-breaking fixed point is an interesting nonperturbative effect as it generates masses for the fermions. The corresponding fixed-point potentials are both global but only in the symmetry-breaking regime the potential is bounded from below. This makes it physically the most valuable one. The mass coupling at the fixed point in the locally symmetric regime is proportional to ϵ whereas the non-trivial minimum of the symmetry-breaking fixed-point potential κ^* is proportional to ϵ^{-2}. It turns out that κ^* is the only coupling that grows when the perturbative limit is increasingly justified. Nevertheless, the radial mass mode connected to the non-trivial minimum via $2\kappa^* \left. u'' \right|_{\rho=\kappa^*}$ and the squared fermion mass are controlled by the Veneziano limit.
In section 4.5 we investigated the critical exponents. At first, the relevant directions for each fixed point which were found perturbatively in [1] are reproduced and corrected: One for the symmetry-breaking fixed point and two for the symmteric one. Beyond that, we have studied the critical exponent corresponding to the mass coupling. It turns out that the associated eigendirection is a relevant one and the exponent differs from two but with decreasing ϵ it reaches its limit two which is also found for the Standard Model.

To summarize our calculations, the Gauge-Yukawa theories exhibit a symmetry-breaking and global potential which is bounded from below and therefore fulfill the consistency criterion for a UV complete QFT. All couplings and quantities except the non-trivial minimum are controlled by the Veneziano limit. From the nonperturbative insights, we can gain new inputs for model building beyond the Stadard Model of particle physics and the Gauge-Yukawa theories might be good candidates for this.

A. Scalar mass spectrum

A.1. Specification to the ρ direction

In this appendix we compute the scalar mass spectrum following from the effective average action (2.44) with a truncated potential U_k depending on the invariants ρ, τ which were defined by

$$\rho = \frac{1}{2}\operatorname{Tr}\phi^2\,, \qquad \tau = \frac{1}{2}\operatorname{Tr}\left(\frac{1}{2}\phi^2 - \frac{\rho}{2N_\mathrm{f}}\right)^2. \tag{A.1}$$

The spectrum constitutes of the two matrices

$$M_{R,cdij} = \frac{\delta^2 U_k}{\delta H_R^{cd}\delta H_R^{ij}}, \qquad M_{I,cdij} = \frac{\delta^2 U_k}{\delta H_I^{cd}\delta H_I^{ij}}, \tag{A.2}$$

with $c,d,i,j \in \{1,..,N_\mathrm{f}\}$ and $H^{ab} = (H_R^{ab} + \mathrm{i}\,H_I^{ab})/\sqrt{2}$. Note that $M_{R,cdij} = \frac{\delta^2 U}{\delta H_R^{cd}\delta H_I^{ij}} = 0$ from which $\left(\Gamma_k^{(2)}\right)_{12} = \left(\Gamma_k^{(2)}\right)_{21} = 0$ results. With the definition (2.17) of $\phi^{\mu\nu}$ ($\mu,\nu \in \{1,..,2N_\mathrm{f}\}$) we obtain the derivatives

$$\frac{\delta\phi^{\mu\nu}}{\delta H_R^{cd}} = \frac{1}{\sqrt{2}}\left(\delta_{\mu c}\delta_{\nu(d+N_\mathrm{f})} + \delta_{\mu(c+N_\mathrm{f})}\delta_{\nu d}\right), \tag{A.3}$$

$$\frac{\delta\phi^{\mu\nu}}{\delta H_I^{cd}} = \frac{i}{\sqrt{2}}\left(\delta_{\mu c}\delta_{\nu(d+N_\mathrm{f})} - \delta_{\mu(c+N_\mathrm{f})}\delta_{\nu d}\right), \tag{A.4}$$

with which we can compute $M_{R,cdij}$ and $M_{I,cdij}$:

$$\begin{aligned} M_{I,cdij} =& \frac{\delta\phi^{ab}}{\delta H_I^{cd}}\frac{\delta^2 U_k}{\delta\phi^{ab}\delta\phi^{rs}}\frac{\delta\phi^{rs}}{\delta H_I^{ij}} \\ =& U_k'\delta_{di}\delta_{cj} + \frac{1}{2}\frac{\partial U_k}{\partial\tau}\left[\delta_{di}\delta_{cj}\varphi_c^2 - \delta_{di}\delta_{cj}\varphi_c\varphi_d + \delta_{di}\delta_{cj}\varphi_d^2 - 8\xi\operatorname{Tr}(\phi^2)\delta_{di}\delta_{cj}\right], \end{aligned} \tag{A.5}$$

$$\begin{aligned} M_{R,cdij} =& \frac{\delta\phi^{ab}}{\delta H_R^{cd}}\frac{\delta^2 U_k}{\delta\phi^{ab}\delta\phi^{rs}}\frac{\delta\phi^{rs}}{\delta H_R^{ij}} \\ =& U_k'\delta_{di}\delta_{cj} + 2U_k''\varphi_d\varphi_i\delta_{dc}\delta_{ji} + \frac{1}{2}\frac{\partial U_k}{\partial\tau}\Big[\delta_{di}\delta_{cj}\varphi_c^2 + \\ &+ \delta_{di}\delta_{cj}\varphi_c\varphi_d + \delta_{di}\delta_{cj}\varphi_d^2 - 8\xi\left(4\varphi_d\varphi_i\delta_{dc}\delta_{ji} + \operatorname{Tr}(\phi^2)\delta_{di}\delta_{cj}\right)\Big], \end{aligned} \tag{A.6}$$

with the abbreviation $\xi = 1/(16N_\mathrm{f})$. In the calculation we have suppressed derivatives of the form $\partial^2 U_k/(\partial\rho\partial\tau)$ and $\partial^2 U_k/(\partial\tau^2)$ due to our truncation (2.18). Since we only evaluate the flow equation on a two dimensional subspace, we choose H to be (2.55)

$$H^{ab} = \frac{1}{\sqrt{2}}(H_R^{ab} + \mathrm{i}\,H_I^{ab}) := m \times \operatorname{diag}(\varepsilon, \underbrace{+1.,..,+1}_{N_\mathrm{f}-1\text{ times}}). \tag{A.7}$$

Hence, we can write

$$H_I^{ab} = 0, \qquad H_R^{ab} = \sqrt{2}\varphi_a \delta^{ab}, \tag{A.8}$$

where no sum over a is understood and $\varphi_1 = m\varepsilon$ $\varphi_i = m$ $(i \neq 1)$. Moreover, for the trace of ϕ^2 follows

$$\mathrm{Tr}\,\phi^2 = 2m^2\left(\varepsilon^2 + N_\mathrm{f} - 1\right). \tag{A.9}$$

The eigenvalues of the matrices (A.5) and (A.6) can now be investigated. We start with (A.5) which turns out to ba a diagonal matrix. Thus, we only need to determine the non-vanishing matrix elements to get the eigenvalues. For that, we distinguish several cases. First, we set $c = d = i = j \equiv a$. We obtain

$$M_{I,a} = U_k' + \frac{1}{2}\frac{\partial U_k}{\partial \tau}\left[\frac{\varphi_a^2}{2} - \frac{m^2}{N_\mathrm{f}}\left(\varepsilon^2 + N_\mathrm{f} - 1\right)\right], \tag{A.10}$$

which results in the eigenvalues

$$a = 1: \qquad \mathfrak{m}_1^2 = U_k' + \frac{1}{2}\frac{\partial U_k}{\partial \tau}(1-\varepsilon^2)\frac{1-N_\mathrm{f}}{N_\mathrm{f}} \qquad \text{degeneracy: } 1, \tag{A.11}$$

$$a \neq 1: \qquad \mathfrak{m}_2^2 = U_k' + \frac{m^2}{2}\frac{\partial U_k}{\partial \tau}\frac{1-\varepsilon^2}{N_\mathrm{f}} \qquad \text{degeneracy: } N_\mathrm{f} - 1. \tag{A.12}$$

In the second case, we set $d = i$ and $c = j$ but $d \neq c$. Hence, we obtain a matrix with two indices:

$$M_{I,cd} = U_k' + \frac{1}{2}\frac{\partial U_k}{\partial \tau}\left(\varphi_c^2 - \varphi_c\varphi_d + \varphi_d^2 - \frac{m^2\left(\varepsilon^2 + N_\mathrm{f} - 1\right)}{N_\mathrm{f}}\right) \tag{A.13}$$

This takes the values

$$c \neq 1, d \neq 1: \qquad \mathfrak{m}_3^2 = U_k' + \frac{m^2}{2}\frac{\partial U_k}{\partial \tau}\frac{1-\varepsilon^2}{N_\mathrm{f}} \qquad \text{degeneracy: } {N_\mathrm{f}}^2 - 3N_\mathrm{f} + 2, \tag{A.14}$$

$$c = 1, d \neq 1: \qquad \mathfrak{m}_4^2 = U_k' + \frac{m^2}{2}\frac{\partial U_k}{\partial \tau}\left(\varepsilon^2 - \varepsilon + \frac{1-\varepsilon^2}{N_\mathrm{f}}\right) \qquad \text{degeneracy: } N_\mathrm{f} - 1, \tag{A.15}$$

$$c \neq 1, d = 1: \qquad \mathfrak{m}_4^2 = U_k' + \frac{m^2}{2}\frac{\partial U_k}{\partial \tau}\left(\varepsilon^2 - \varepsilon + \frac{1-\varepsilon^2}{N_\mathrm{f}}\right) \qquad \text{degeneracy: } N_\mathrm{f} - 1, \tag{A.16}$$

such that we end up with ${N_\mathrm{f}}^2$ eigenvalues of $M_{I,cdij}$ as we should. The degeneracy in the upper case ($c \neq 1, d \neq 1$) emerges since we have $N_\mathrm{f} - 1$ possibilities to choose c and then $N_\mathrm{f} - 2$ to choose d. The same calculations can be done for (A.6). This matrix has most of its non-vanishing elements on the diagonal except for a few ones which we determine at the end (they are proportional to $\delta_{cd}\delta_{ij}$). We start with the case $d = i$, $j = c$ but $i \neq j$ where we find a diagonal, symmetric matrix

$$M_{R,cd} = U_k' + \frac{m^2}{2}\frac{\partial U_k}{\partial \tau}\left(\varphi_c^2 + \varphi_d\varphi_c + \varphi_d^2 - \frac{m^2\left(\varepsilon^2 + N_\mathrm{f} - 1\right)}{N_\mathrm{f}}\right), \tag{A.17}$$

with non-vanishing elements

$$c = 1, d \neq 1 \vee c \neq 1, d = 1: \qquad \mathfrak{m}_5^2 = U_k' + \frac{m^2}{2}\frac{\partial U_k}{\partial \tau}\left(\varepsilon^2 + \varepsilon + \frac{1-\varepsilon^2}{N_\mathrm{f}}\right) \qquad \text{degeneracy: } 2N_\mathrm{f} - 2, \tag{A.18}$$

$$c \neq 1, d \neq 1, c \neq d: \qquad \mathfrak{m}_6^2 = U_k' + \frac{m^2}{2}\frac{\partial U_k}{\partial \tau}\left(2 + \frac{1-\varepsilon^2}{N_\mathrm{f}}\right) \qquad \text{degeneracy: } {N_\mathrm{f}}^2 - 3N_\mathrm{f} + 2. \tag{A.19}$$

In the last case $d = c, i = j$ we find a $N_\mathrm{f} \times N_\mathrm{f}$ submatrix where every entry is unequal to zero. It has the form

$$M_{R,di} = U_k' \delta_{di} + 2U_k'' m^2 \varepsilon^2 + \frac{m^2}{2} \frac{\partial U_k}{\partial \tau} \left[3\varphi_d^2 \delta_{di} - 8\xi \left(4\varphi_d \varphi_i + 2m^2 (\varepsilon^2 + N_\mathrm{f} - 1) \right) \delta_{di} \right], \tag{A.20}$$

which we write down in matrix form as

$$\widetilde{M}_R = \begin{pmatrix} a & d\varepsilon & \cdots & \cdots & d\varepsilon \\ d\varepsilon & b & d & \cdots & d \\ \vdots & d & \ddots & \ddots & \vdots \\ \vdots & \vdots & \ddots & \ddots & d \\ d\varepsilon & d & \cdots & d & b \end{pmatrix} \tag{A.21}$$

with

$$\begin{aligned} a =& U_k' - \mathfrak{m}^2 + 2U_k'' m^2 \varepsilon^2 + \frac{m^2}{2} \frac{\partial U_k}{\partial \tau} \left[3\varepsilon^2 - \frac{1}{N_\mathrm{f}} \left(2\varepsilon^2 + (\varepsilon^2 + N_\mathrm{f} - 1) \right) \right], \\ b =& U_k' - \mathfrak{m}^2 + 2U_k'' m^2 + \frac{m^2}{2} \frac{\partial U_k}{\partial \tau} \left[3 - \frac{1}{N_\mathrm{f}} (2 + \varepsilon^2 + N_\mathrm{f} - 1) \right], \\ d =& 2U_k'' m^2 - \frac{m^2}{N_\mathrm{f}} \frac{\partial U_k}{\partial \tau}, \end{aligned}$$

where we have already substracted the eigenvalues $\mathfrak{m}^2$ on the diagonal of $\widetilde{M}_R$. To compute the determinant of such a matrix we write $\widetilde{M}_R := S + \vec{u} \cdot \vec{v}^\mathrm{T}$ with

$$S := \mathrm{diag}(a - d\varepsilon^2, b - d, .., b - d), \qquad \vec{u} = (\varepsilon, 1, .., 1)^\mathrm{T}, \qquad \vec{v} = d(\varepsilon, 1, .., 1)^\mathrm{T}, \tag{A.22}$$

which can be shown easily. This is useful since the determinant of such a matrix can be evaluated with

$$\det \widetilde{M}_R = \det \left(S + \vec{u} \cdot \vec{v}^\mathrm{T} \right) = \left(1 + \vec{v}^\mathrm{T} S^{-1} \vec{u} \right) \det S, \tag{A.23}$$

which is proved e.g. in [40]. This is much easier since S is a diagonal matrix. We find

$$\det \widetilde{M}_R = (b-d)^{N_\mathrm{f}-2} \left[(a - d\varepsilon^2)(b-d) + d\varepsilon^2 (b-d) + d(N_\mathrm{f} - 1)(a - d\varepsilon^2) \right] \stackrel{!}{=} 0, \tag{A.24}$$

which has the solutions

$$\begin{aligned} \mathfrak{m}_{7,8}^2 =& U_k' + \frac{m^2}{4N_\mathrm{f}} \Big\{ 4N_\mathrm{f}(N_\mathrm{f} - 1) U_k'' + (4 - N_\mathrm{f}) U_{k,\tau} + \left[4N_\mathrm{f} U_k'' + (3N_\mathrm{f} - 4) U_{k,\tau} \right] \varepsilon^2 \\ & \pm \Big[\left(4N_\mathrm{f}(N_\mathrm{f} - 1) U_k'' + (N_\mathrm{f} + 2) U_{k,\tau} \right)^2 + 2 \big(16 {N_\mathrm{f}}^2 (N_\mathrm{f} - 1) {U_k''}^2 - 4N_\mathrm{f}(N_\mathrm{f} + 2)(3N_\mathrm{f} - 2) U_k'' U_{k,\tau} \\ & - (3{N_\mathrm{f}}^2 - 4N_\mathrm{f} + 4) U_{k,\tau}^2 \big) \varepsilon^2 + \left(4N_\mathrm{f} U_k'' + (3N_\mathrm{f} - 2) U_{k,\tau} \right)^2 \varepsilon^4 \Big]^{1/2} \Big\}, \end{aligned} \tag{A.25}$$

with degeneracy 1 + 1 (we abbreviated $U_{k,\tau} = \partial U_k / \partial \tau$) and

$$\mathfrak{m}_9^2 = U_k' + \frac{m^2}{2} \frac{\partial U_k}{\partial \tau} \left(2 + \frac{1 - \varepsilon^2}{N_\mathrm{f}} \right), \tag{A.26}$$

which is $N_\mathrm{f} - 2$ times degenerated. In summary, we find the scalar mass spectrum of table 2.1 which has $2{N_\mathrm{f}}^2$ eigenvalues in total as we should starting with a complex $N_\mathrm{f} \times N_\mathrm{f}$ scalar field H.

A.2. Generalization including second derivatives in τ direction

Up to now we have set

$$\frac{\partial^2 U_k}{\partial\rho\partial\tau} = \frac{\partial^2 U_k}{\partial\tau^2} = 0, \tag{A.27}$$

since our truncated potential was of the form (2.18) and did not contain any mixed terms of ρ and τ or higher order τ terms. To be able to compute fixed-point potentials in the τ direction, we need to include a term of the form $\lambda_3\tau^2/2$ into our truncation of the potential. This of course changes the mass spectrum of scalar fluctuations. Computations work analogously as in appendix A.1. We obtain

$$M_{I,cdij} = U_k'\delta_{di}\delta_{cj} + \frac{1}{2}\frac{\partial U_k}{\partial\tau}\left[\delta_{di}\delta_{cj}\varphi_c^2 - \delta_{di}\delta_{cj}\varphi_c\varphi_d + \delta_{di}\delta_{cj}\varphi_d^2 - 8\xi\,\mathrm{Tr}(\phi^2)\delta_{di}\delta_{cj}\right], \tag{A.28}$$

$$\begin{aligned} M_{R,cdij} = {} & U_k'\delta_{di}\delta_{cj} + 2U_k''\varphi_d\varphi_i\delta_{dc}\delta_{ji} + \frac{1}{2}\frac{\partial U_k}{\partial\tau}\Big[\delta_{di}\delta_{cj}\left(\varphi_c^2 + \varphi_c\varphi_d + \varphi_d^2\right) + \\ & - 8\xi\left(4\varphi_d\varphi_i\delta_{dc}\delta_{ji} + \mathrm{Tr}(\phi^2)\delta_{di}\delta_{cj}\right)\Big] + \\ & + \frac{1}{2}\frac{\partial^2 U_k}{\partial\tau^2}\left[\varphi_c^3\varphi_i^3 - 8\xi\,\mathrm{Tr}(\phi^2)\left(\varphi_c\varphi_i^3 - \varphi_c^3\varphi_i\right) + \left(8\xi\,\mathrm{Tr}(\phi^2)\right)^2\varphi_c\varphi_i\right]\delta_{cd}\delta_{ij}. \end{aligned} \tag{A.29}$$

All eigenvalues that do not include any second derivatives of U_k remain unchanged. Hence, only the eigenvalues $\mathfrak{m}_{7,8}^2$ will change. We can compute those eigenvalues with the same machinery (A.23) as above. This time we introduce the abbreviations

$$\begin{aligned} a &= U_k' - \mathfrak{m}^2 + 2U_k''m^2\varepsilon^2 + \frac{m^2}{2}\frac{\partial U_k}{\partial\tau}\left[3\varepsilon^2 - \frac{1}{N_\mathrm{f}}\left(2\varepsilon^2 + (\varepsilon^2 + N_\mathrm{f} - 1)\right)\right] + \frac{m^6}{2}\frac{\partial^2 U_k}{\partial\tau^2}\left(\varepsilon^6 + \frac{\varepsilon^2}{N_\mathrm{f}^2}(\varepsilon^2 + N_\mathrm{f} - 1)^2\right), \\ b &= U_k' - \mathfrak{m}^2 + 2U_k''m^2 + \frac{m^2}{2}\frac{\partial U_k}{\partial\tau}\left[3 - \frac{1}{N_\mathrm{f}}(2 + \varepsilon^2 + N_\mathrm{f} - 1)\right] + \frac{m^6}{2}\frac{\partial^2 U_k}{\partial\tau^2}\left(1 + \frac{1}{N_\mathrm{f}^2}(\varepsilon^2 + N_\mathrm{f} - 1)^2\right), \\ e &= 2U_k''m^2 - \frac{m^2}{N_\mathrm{f}}\frac{\partial U_k}{\partial\tau} + \frac{m^6}{2N_\mathrm{f}^2}\frac{\partial^2 U_k}{\partial\tau^2}(\varepsilon^2 + N_\mathrm{f} - 1)^2, \\ f &= \frac{m^6}{2N_\mathrm{f}}\frac{\partial^2 U_k}{\partial\tau^2}(\varepsilon^2 + N_\mathrm{f} - 1)(\varepsilon^3 - \varepsilon), \\ g &= \frac{m^6}{2}\frac{\partial^2 U_k}{\partial\tau^2}, \end{aligned}$$

such that we write the submatrix where no entry vanishes (all other eigenvalues are independent of second derivatives) as

$$\widetilde{M}_R = \begin{pmatrix} a & e\varepsilon + g\varepsilon^3 + f & \cdots & \cdots & e\varepsilon + g\varepsilon^3 + f \\ e\varepsilon + g\varepsilon^3 - f & b & e+g & \cdots & e+g \\ \vdots & e+g & \ddots & \ddots & \vdots \\ \vdots & \vdots & \ddots & \ddots & e+g \\ e\varepsilon + g\varepsilon^3 - f & e+g & \cdots & e+g & b \end{pmatrix}. \tag{A.30}$$

Following the line of reasoning from above, we split um $\widetilde{M}_R$ into $\widetilde{M}_R \coloneqq S + \vec{u}\cdot\vec{v}^{\mathrm{T}}$ with

$$S = \begin{pmatrix} a-e\varepsilon^2-g\varepsilon^2 & g\varepsilon^3-g\varepsilon+f & \cdots & \cdots & g\varepsilon^3-g\varepsilon+f \\ g\varepsilon^3-g\varepsilon-f & b-e-g & 0 & \cdots & 0 \\ \vdots & 0 & \ddots & \ddots & \vdots \\ \vdots & \vdots & \ddots & \ddots & 0 \\ g\varepsilon^3-g\varepsilon-f & 0 & \cdots & 0 & b-e-g \end{pmatrix}, \tag{A.31}$$

$\vec{u} = (\varepsilon, 1, .., 1)^{\mathrm{T}}$ and $\vec{v} = (e+g)(\varepsilon, 1, .., 1)^{\mathrm{T}}$. The inverse of S reads

$$\widetilde{M}_R = \frac{1}{\xi}\begin{pmatrix} \alpha & \gamma & \cdots & \cdots & \gamma \\ \zeta & \beta & \varkappa & \cdots & \varkappa \\ \vdots & \varkappa & \ddots & \ddots & \vdots \\ \vdots & \vdots & \ddots & \ddots & \varkappa \\ \zeta & \varkappa & \cdots & \varkappa & \beta \end{pmatrix}, \tag{A.32}$$

with

$$\begin{aligned}
\xi &= (N_{\mathrm{f}}-1)(b-e-g)^{N_{\mathrm{f}}-2}\left[-(g\varepsilon^3-g\varepsilon)^2+f^2\right] + (a-e\varepsilon^2-g\varepsilon^2)(b-e-g)^{N_{\mathrm{f}}-1}, \\
\alpha &= (b-e-g)^{N_{\mathrm{f}}-1}, \\
\beta &= (N_{\mathrm{f}}-2)(b-e-g)^{N_{\mathrm{f}}-3}\left[-(g\varepsilon^3-g\varepsilon)^2+f^2\right] + (a-e\varepsilon^2-g\varepsilon^2)(b-e-g)^{N_{\mathrm{f}}-2}, \\
\gamma &= -(b-e-g)^{N_{\mathrm{f}}-2}(g\varepsilon^3-g\varepsilon+f), \\
\zeta &= (b-e-g)^{N_{\mathrm{f}}-2}\left(-(g\varepsilon^3-g\varepsilon)+f\right), \\
\varkappa &= (b-e-g)^{N_{\mathrm{f}}-3}\left((g\varepsilon^3-g\varepsilon)^2-f^2\right).
\end{aligned}$$

Evaluating the determinant ends in

$$\begin{aligned}
\det\widetilde{M}_R = (b-e-g)^{N_{\mathrm{f}}-2}\Big[&(N_{\mathrm{f}}-1)(f^2-(g\varepsilon^3-g\varepsilon)^2) + (a-e\varepsilon^2-g\varepsilon^2)(b-e-g) + \\
&+ (e+g)\left((b-e-g)\varepsilon^2 + (N_{\mathrm{f}}-1)\left(-2\varepsilon(g\varepsilon^3-g\varepsilon) + (a-e\varepsilon^2-g\varepsilon^2)\right)\right)\Big] \stackrel{!}{=} 0,
\end{aligned}$$

where we find as before (if $(b-e-g)^{N_{\mathrm{f}}-2}$ vanishes)

$$\mathfrak{m}_9^2 = U_k' + \frac{m^2}{2}\frac{\partial U_k}{\partial\tau}\left(2+\frac{1-\varepsilon^2}{N_{\mathrm{f}}}\right), \tag{A.33}$$

$N_\mathrm{f}-2$ degenerated. If the squared brackets in (A.33) vanish we find the non-degenerated eigenvalues

$$\begin{aligned}
\mathfrak{m}_{7,8}^2 =& U' + \frac{1}{4}\Big(\frac{m^6 U_{\tau\tau}\left(2{N_\mathrm{f}}^3 + {N_\mathrm{f}}^2\left(\varepsilon^6+3\varepsilon^2-4\right) + 3N_\mathrm{f}\left(\varepsilon^2-1\right)^2 + \left(\varepsilon^2-1\right)^3\right)}{{N_\mathrm{f}}^2} \\
&+ \frac{m^2\left(4N_\mathrm{f}\left(N_\mathrm{f}+\varepsilon^2-1\right)U'' + U_\tau\left((3N_\mathrm{f}-4)\varepsilon^2 - N_\mathrm{f}+4\right)\right)}{N_\mathrm{f}} \pm \frac{m^2}{{N_\mathrm{f}}^2}\Big[4m^8 {N_\mathrm{f}}^6 U_{\tau\tau}^2 + m^8 U_{\tau\tau}^2\left(\varepsilon^2-1\right)^6 \\
&- 4m^4 {N_\mathrm{f}}^5 U_{\tau\tau}\left(m^4 U_{\tau\tau}\left(\varepsilon^6-4\varepsilon^4-\varepsilon^2+4\right) + U_\tau\left(3\varepsilon^2-1\right)\right) + 8{N_\mathrm{f}}^2 U''\left(2m^4 {N_\mathrm{f}}^4 U_{\tau\tau}\right. \\
&+ {N_\mathrm{f}}^3\left(m^4(-U_{\tau\tau})\left(\varepsilon^6-4\varepsilon^4-3\varepsilon^2+6\right) - 3U_\tau\varepsilon^2 + U_\tau\right) + {N_\mathrm{f}}^2\left(\varepsilon^2-1\right)\left(m^4 U_{\tau\tau}\left(\varepsilon^6+2\varepsilon^4+4\varepsilon^2-7\right)\right. \\
&\left.\left.+ U_\tau\left(3\varepsilon^2-1\right)\right) - 2N_\mathrm{f}\left(\varepsilon^2-1\right)^2\left(U_\tau - 2m^4 U_{\tau\tau}\left(\varepsilon^2-1\right)\right) + m^4 U_{\tau\tau}\left(\varepsilon^2-1\right)^4\right) + 2m^4 N_\mathrm{f} U_{\tau\tau}\left(\varepsilon^2-1\right)^4 \\
&\times\left(3m^4 U_{\tau\tau}\left(\varepsilon^2-1\right) - 2U_\tau\right) + {N_\mathrm{f}}^4\left(m^8 U_{\tau\tau}^2\left(\varepsilon^2-1\right)^2\left(\varepsilon^8+2\varepsilon^6-7\varepsilon^4+32\varepsilon^2+28\right)\right. \\
&+ 2m^4 U_\tau U_{\tau\tau}\varepsilon^2\left(3\varepsilon^6-\varepsilon^4-11\varepsilon^2+9\right) + U_\tau^2\left(1-3\varepsilon^2\right)^2\Big) - 2{N_\mathrm{f}}^3\left(\varepsilon^2-1\right)\Big(m^8 U_{\tau\tau}^2\left(\varepsilon^2-1\right)^2\left(\varepsilon^4-15\varepsilon^2-14\right) \\
&+ m^4 U_\tau U_{\tau\tau}\left(2\varepsilon^6+\varepsilon^4+2\varepsilon^2-5\right) + U_\tau^2\left(6\varepsilon^2+2\right)\Big) + {N_\mathrm{f}}^2\left(\varepsilon^2-1\right)^2\Big(m^8 U_{\tau\tau}^2\left(\varepsilon^2-1\right)^2\left(2\varepsilon^4+10\varepsilon^2+17\right) \\
&\left.+ 2m^4 U_\tau U_{\tau\tau}\left(3\varepsilon^4-8\varepsilon^2+5\right) + 4U_\tau^2\right) + 16{N_\mathrm{f}}^4\left(N_\mathrm{f}+\varepsilon^2-1\right)^2\left(U''\right)^2\Big]^{1/2}\Big),
\end{aligned}$$

which simplifies to (A.25) when setting $U_{\tau\tau}=0$. We have suppressed the subscript k of the potential and wrote subscript τ for the derivative with respect to τ.

B. Threshold functions with linear cut-off

In this chapter we provide the definitions of the threshold integrals used in section 2.3.2 and explicit results when a linear cut-off is applied. We have already introduced the abbreviations

$$P(p) = p^2\left(1 + r_{kB}(p)\right), \tag{B.1}$$

$$P_F(p) = p^2\left(1 + r_{kF}(p)\right)^2, \tag{B.2}$$

$$v_d^{-1} = 2^{d+1}\pi^{d/2}\Gamma(d/2), \tag{B.3}$$

such that we can define the threshold functions by[1] (see e.g. [28], [29], [21])

$$l_n^d(\omega;\eta_\phi) = \frac{n+\delta_{n,0}}{4} v_d^{-1} k^{2n-d} \int_q \left[\left(\frac{1}{Z_\phi}\frac{\partial R_K(q)}{\partial t}\right)\left(P(q)+\omega k^2\right)^{-(n+1)}\right], \tag{B.4}$$

$$l_n^{(F)d}(\omega;\eta_\chi) = \frac{n+\delta_{n,0}}{2} v_d^{-1} k^{2n-d} \int_q \left[\frac{P_F(q)}{1+r_{kF}(q)}\left(\frac{1}{Z_\chi}\frac{\partial\left(Z_\chi r_{kF}\right)}{\partial t}\right)\left(P_F(q)+\omega k^2\right)^{-(n+1)}\right]. \tag{B.5}$$

The linear cut-off has the explicit form

$$r_{kB}^{\text{lin}}(p) = \left(\frac{k^2}{p^2} - 1\right)\Theta\left(1 - \frac{p^2}{k^2}\right) \tag{B.6}$$

with $(1 + r_{kB}^{\text{lin}}(p)) = (1 + r_{kF}^{\text{lin}}(p))^2$ and has the big advantage that the threshold integrals can be integrated analytically [16]. We get

$$l_n^d\left(\omega;\eta_\phi\right) = \frac{2\left(\delta_{n,0}+n\right)}{d}\left(1 - \frac{\eta_\phi}{d+2}\right)\frac{1}{(1+\omega)^{n+1}}, \tag{B.7}$$

$$l_n^{(F)d}\left(\omega;\eta_\chi\right) = \frac{2\left(\delta_{n,0}+n\right)}{d}\left(1 - \frac{\eta_\chi}{d+1}\right)\frac{1}{(1+\omega)^{n+1}}, \tag{B.8}$$

$$l_{n_1,n_2}^d(\omega_1,\omega_2;\eta_\phi) = \frac{2}{d}\left(1 - \frac{\eta_\phi}{d+2}\right)\left(\frac{n_1}{1+\omega_1} + \frac{n_2}{1+\omega_2}\right)\frac{1}{(1+\omega_1)^{n_1}(1+\omega_2)^{n_2}}, \tag{B.9}$$

$$m_{n_1,n_2}^d\left(\omega_1,\omega_2;\eta_\phi\right) = \frac{1}{(1+\omega_1)^{n_1}(1+\omega_2)^{n_2}}, \tag{B.10}$$

$$m_4^{(F)d}\left(\omega;\eta_\chi\right) = \frac{1}{(1+\omega)^4} + \frac{1-\eta_\chi}{d-2}\frac{1}{(1+\omega)^3} - \left(\frac{1-\eta_\chi}{2d-4} + \frac{1}{4}\right)\frac{1}{(1+\omega)^2}, \tag{B.11}$$

$$m_{n_1,n_2}^{(FB)d}\left(\omega_1,\omega_2;\eta_\chi,\eta_\phi\right) = \left(1 - \frac{\eta_\phi}{d+1}\right)\frac{1}{(1+\omega_1)^{n_1}(1+\omega_2)^{n_2}}. \tag{B.12}$$

[1] We mention here only the two integrals that we explicitly use. The definitions for the other integrals which we only use after applying the linear cut-off can be found e.g. in [28], [29], [21].

Bibliography

[1] Daniel F. Litim and Francesco Sannino. Asymptotic safety guaranteed. *Journal of High Energy Physics*, 2014(12), Dec 2014. ISSN 1029-8479. arXiv:1406.2337 [hep-th].

[2] Kenneth G. Wilson. Renormalization Group and Critical Phenomena. I. Renormalization Group and the Kadanoff Scaling Picture. *Phys. Rev. B*, 4:3174–3183, Nov 1971. 10.1103/PhysRevB.4.3174.

[3] Kenneth G. Wilson. Renormalization Group and Critical Phenomena. II. Phase-Space Cell Analysis of Critical Behavior. *Phys. Rev. B*, 4:3184–3205, Nov 1971. 10.1103/PhysRevB.4.3184.

[4] M. Reuter and F. Saueressig. Quantum Einstein Gravity. *New Journal of Physics focus issue on Quantum Einstein Gravity*, Feb 2012. arXiv:1202.2274 [hep-th].

[5] Holger Gies, Stefan Rechenberger, Michael M. Scherer, and Luca Zambelli. An asymptotic safety scenario for gauged chiral Higgs–Yukawa models. *The European Physical Journal C*, 73(12), Nov 2013. ISSN 1434-6052. arXiv:0907.0327 [hep-th].

[6] Holger Hies, Joerg Jaeckel, and Christof Wetterich. Toward a renormalizable standard model without fundamental higgs scalar. *Phys. Rev. D*, 69:18, 2004. arXiv:hep-ph/0312034.

[7] S. Weinberg, S. W. Hawking, and W. Israel. *General Relativity: An Einstein centenary survey*. Cambridge University Press, 1979.

[8] O. Zanusso, L. Zambelli, G. P. Vacca, and R. Percacci. Gravitational corrections to Yukawa systems. *Physics Letters B*, 689:90–94, May 2010. arXiv:0904.0938 [hep-th].

[9] L. D. Landau. *Niels Bohr and the Development of Physics*. Pergamon Press, London, 1955.

[10] Holger Gies and Joerg Jaeckel. Renormalization Flow of QED. *Physical Review Letters*, 93 (11), Sep 2004. ISSN 1079-7114. arXiv:hep-ph/0405183.

[11] Steven Weinberg. Critical Phenomena for Field Theorists. In *14th International School of Subnuclear Physics: Understanding the Fundamental Constitutents of Matter*, page 1, 8 1976.

[12] Marie E. Machacek and Michael T. Vaughn. Two-loop renormalization group equations in a general quantum field theory: (I). Wave function renormalization. *Nuclear Physics B*, 222 (1):83–103, Feb 1983. DOI:10.1016/0550-3213(83)90610-7.

[13] Marie E. Machacek and Michael T. Vaughn. Two-loop renormalization group equations in a general quantum field theory: (II). Yukawa couplings. *Nuclear Physics B*, 236(1):221–232, Feb 1983. DOI:10.1016/0550-3213(84)90533-9.

[14] Marie E. Machacek and Michael T. Vaughn. Two-loop renormalization group equations in a general quantum field theory: (III). Scalar quartic couplings. *Nuclear Physics B*, 249(1): 70–92, Jan 1985. DOI:10.1016/0550-3213(85)90040-9.

[15] Christof Wetterich. Exact evolution equation for the effective potential. *Phys. Lett. B*, 301: 90–94, 1993. DOI:10.1016/0370-2693(93)90726-X.

[16] Daniel F. Litim. Critical exponents from optimised renormalisation group flows. *Nuclear Physics B*, 631(1-2):128–158, Jun 2002. ISSN 0550-3213. arXiv:hep-th/0203006.

[17] Andreas Wipf. *Statistical Approach to Quantum Field Theory: An Introduction*. Springer Verlag, 2013. ISBN 978-3-642-33105-3.

[18] L. Dabelow. Global analytic approximation to the Wilson-Fisher fixed-point potential, University of Jena 2015. Thesis.

[19] J. Borchardt and B. Knorr. Global solutions of functional fixed point equations via pseudospectral methods. *Physical Review D*, 91(10), May 2015. ISSN 1550-2368. arXiv:150207511v2[hep-th].

[20] Jens Braun, Holger Gies, and Daniel D. Scherer. Asymptotic safety: A simple example. *Physical Review D*, 83(8), Apr 2011. ISSN 1550-2368. arXiv:1011.1456 [hep-th].

[21] C. Gneiting. Higgs mass bounds from renormalization flow, University of Heidelberg 2011. Thesis.

[22] M. Ansorg, A. Kleinwächter, and R. Meinel. Highly accurate calculation of rotating neutron stars. *Astronomy and Astrophysics*, 405(2):711–721, Jun 2003. ISSN 1432-0746. arXiv:astro-ph/0301173.

[23] Daniel F. Litim and Lautaro Vergara. Subleading critical exponents from the renormalisation group. *Physics Letters B*, 581(3-4):263–269, Feb 2004. ISSN 0370-2693. arXiv:hep-th/0310101.

[24] M. E. Peskin and D. V. Schroeder. *Introduction To Quantum Field Theory*. Taylor and Francis Inc., 1995. ISBN 978-0-201-50397-5.

[25] Holger Gies. Introduction to the Functional RG and Applications to Gauge Theories. *Lecture Notes in Physics*, page 287–348, 2012. ISBN 9783642273209. ISSN 1616-6361. arXiv:hep-ph/0611146 [hep-th].

[26] Astrid Eichhorn. *Quantum fields in the non-perturbative regime - Yang-Mills theory and gravity*. PhD thesis, Friedrich-Schiller-Universität Jena, 2011. PhD Thesis.

[27] Michael M. Scherer. *Introduction to Renormalization*. Institut for Theoretical Physics, University of Cologne, 2017. Link to Lecture.

[28] Lukas Janssen and Holger Gies. Critical behavior of the (2+1)-dimensional Thirring model. *Physical Review D*, 86(10), Nov 2012. ISSN 1550-2368. arXiv:1208.3327 [hep-th].

[29] D.-U. Jungnickel and C. Wetterich. Effective action for the chiral quark-meson model. *Physical Review D*, 53(9):5142–5175, May 1996. ISSN 1089-4918. arXiv:hep-ph/9505267[hep-th].

[30] K. Osterwalder and R. Schrader. Axioms for Euclidean Green's functions. *Communications in Mathematical Physics*, 31(2):83–112, Jun 1973. 10.1007/BF01645738.

[31] K. Osterwalder and R. Schrader. Axioms for Euclidean Green's functions II. *Communications in Mathematical Physics*, 42(3):281–305, Oct 1975. 10.1007/BF01608978.

[32] Holger Gies and Luca Zambelli. Non-Abelian Higgs models: Paving the way for asymptotic freedom. *Physical Review D*, 96(2), Jul 2017. ISSN 2470-0029. arXiv:1611.09147 [hep-ph].

[33] Holger Gies, Clemens Gneiting, and René Sondenheimer. Higgs mass bounds from renormalization flow for a simple Yukawa model. *Physical Review D*, 89(4), Feb 2014. ISSN 1550-2368. arXiv:1308.5075 [hep-ph].

[34] C. Bervillier, B. Boisseau, and H. Giacomini. Analytical approximation schemes for solving exact renormalization group equations in the local potential approximation. *Nuclear Physics B*, 789(3):525–551, Feb 2008. ISSN 0550-3213. arXiv:0706.0990 [hep-th].

[35] Tim R. Morris. Elements of the Continuous Renormalization Group. *Progress of Theoretical Physics Supplement*, 131:395–414, 1998. ISSN 0375-9687. arXiv:hep-th/9802039.

[36] Tobias Hellwig, Andreas Wipf, and Omar Zanusso. Scaling and superscaling solutions from the functional renormalization group. *Physical Review D*, 92(8), Oct 2015. ISSN 1550-2368. arXiv:1508.02547[hep-th].

[37] Robert E. Robson and Prytz Arnstein. The discrete ordinate/pseudo-spectral method: review and application from a physicist's perspective. *Australian journal of physics*, 46(4): 465–496, 1993.

[38] Christian S Fischer and Holger Gies. Renormalization flow of yang-mills propagators. *Journal of High Energy Physics*, 2004(10):048–048, Oct 2004. ISSN 1029-8479. arXiv:hep-ph/0408089.

[39] J. P. Boyd. *Chebyshev and Fourier Spectral Methods*. Dover Publications, 2000.

[40] Philip D. Powell. Calculating Determinants of Block Matrices, 2011. arXiv:1112.4379[math.RA] .

Danksagung

Zuallererst möchte ich mich ganz herzlich bei meinem Betreuer Professor Holger Gies bedanken. Sie haben mir die Möglichkeit gegeben, meine Masterarbeit auf einem sehr interessanten Gebiet zu schreiben und haben sich immer Zeit für alle meine Fragen und Probleme genommen. Durch Ihr Interesse am Thema und meinen Ergebnissen hätte ich mir keine bessere Betreuung wünschen können.
Außerdem bedanke ich mich bei Luca Zambelli für die Übernahme der Zweitkorrektur und bei Benjamin Knorr sowie Luca Zambelli für die wertvollen Diskussionen zur pseudo-spektralen Methode. Meinem Vater Christian Müller und Richard Schmieden danke ich für das Korrekturlesen. Nicht zuletzt möchte ich meinen Kollegen Richard Schmieden und Ruben Küspert für die vielen Diskussionen danken.
Natürlich gilt mein ganz großer Dank auch meiner Familie für die jahrelange Unterstützung im gesamten Studium und allen anderen Entscheidungen.

Selbstständigkeit und Veröffentlichung

Ich erkläre, die vorliegende Arbeit selbstständig verfasst, und keine anderen als die angegebenen Quellen und Hilfsmittel verwendet zu haben.

Vonseiten des Verfassers bestehen keinerlei Einwände, diese Arbeit der Thüringer Universitäts- und Landesbibliothek zur öffentlichen Nutzung zur Verfügung zu stellen.

Jena, den 17. September 2020

Simon Schreyer